

# The role of GABARAPL1/GEC1 in autophagic flux and mitochondrial quality control in MDA-MB-436 breast cancer cells

Michaël Boyer-Guittaut,<sup>1,2,3,\*</sup> Laura Poillet,<sup>1</sup> Qiuli Liang,<sup>2,3</sup> Elodie Bôle-Richard,<sup>1,†</sup> Xiaosen Ouyang,<sup>2,3,4</sup> Gloria A Benavides,<sup>2,3</sup> Fatima-Zahra Chakrama,<sup>1,‡</sup> Annick Fraichard,<sup>1</sup> Victor M Darley-USmar,<sup>2,3</sup> Gilles Despouy,<sup>1</sup> Michèle Jouvenot,<sup>1</sup> Régis Delage-Mourroux,<sup>1</sup> and Jianhua Zhang<sup>2,3,4,\*</sup>

<sup>1</sup>Université de Franche-Comté; Laboratoire de Biochimie; EA3922 Estrogènes; Expression Génique et Pathologies du Système Nerveux Central; Sciences et Techniques; Besançon, France; <sup>2</sup>Department of Pathology; University of Alabama at Birmingham; Birmingham, AL USA; <sup>3</sup>Center for Free Radical Biology; University of Alabama at Birmingham; Birmingham, AL USA; <sup>4</sup>Department of Veterans Affairs; Birmingham VA Medical Center; Birmingham, AL USA

Current affiliation: <sup>†</sup>EFS B/F-C; INSERM; Interactions Hôte-Greffon-Tumeurs & Ingénierie Cellulaire et Génique; Besançon, France; <sup>‡</sup>Université de Lyon; Inserm U1052; Centre de Recherche en Cancérologie de Lyon; Centre Léon Bérard; Lyon, France

**Keywords:** autophagy, breast cancer, GABARAP, GABARAPL1, GEC1, LAMP1, LC3, lysosome, MDA-MB-436, mitochondria, mitophagy

**Abbreviations:** ATG, autophagy-related; CQ, chloroquine; BafA1, bafilomycin A<sub>1</sub>; DNML/Drp1, dynamin 1-like; ECAR, extracellular acidification rate; FCCP, carbonyl cyanide 4-(trifluoromethoxy)phenylhydrazone; GABA, gamma-aminobutyric acid; GABA<sub>A</sub>R, gamma-aminobutyric acid type A receptor; GABARAP, GABA(A)receptor-associated protein; GABARAPL1/GEC1, GABA(A) receptor-associated protein like 1; GABARAPL2/GATE-16, GABA(A) receptor-associated protein-like 2; GFP, green fluorescent protein; GSH, glutathione; HNE, 4-hydroxynonenal; KD, knockdown; MAP1LC3, microtubule-associated protein 1 light chain 3; MFN1, mitofusin 1; MTT, 3-(4,5-dimethylthiazol-2-yl)-2,5-diphenyl tetrazolium bromide; NBR1, neighbor of BRCA1 gene 1; OCR, oxygen consumption rate; PBS, phosphate-buffered saline; PBS-T, PBS-Triton-X; PFA, paraformaldehyde; PPARGC1A, peroxisome proliferator-activated receptor gamma, coactivator 1alpha; PINK1, PTEN-induced putative kinase 1; PVDF, polyvinylidenedifluoride; RCR, respiratory control ratio; SDS, sodium dodecylsulfate; SQSTM1/p62, sequestosome 1; TBS-T, Tris buffered saline-Tween; TMRM, tetramethylrhodamine methyl ester perchlorate; VDACL1, voltage-dependent anion channel 1; WT, wild type

*GABARAPL1/GEC1* is an early estrogen-induced gene which encodes a protein highly conserved from *C. elegans* to humans. Overexpressed GABARAPL1 interacts with GABA<sub>A</sub> or kappa opioid receptors, associates with autophagic vesicles, and inhibits breast cancer cell proliferation. However, the function of endogenous GABARAPL1 has not been extensively studied. We hypothesized that GABARAPL1 is required for maintaining normal autophagic flux, and plays an important role in regulating cellular bioenergetics and metabolism. To test this hypothesis, we knocked down *GABARAPL1* expression in the breast cancer MDA-MB-436 cell line by shRNA. Decreased expression of GABARAPL1 activated pro-cancer responses of the MDA-MB-436 cells including increased proliferation, colony formation, and invasion. In addition, cells with decreased expression of GABARAPL1 exhibited attenuated autophagic flux and a decreased number of lysosomes. Moreover, decreased GABARAPL1 expression led to cellular bioenergetic changes including increased basal oxygen consumption rate, increased intracellular ATP, increased total glutathione, and an accumulation of damaged mitochondria. Taken together, our results demonstrate that GABARAPL1 plays an important role in cell proliferation, invasion, and autophagic flux, as well as in mitochondrial homeostasis and cellular metabolic programs.

## Introduction

The *GABARAPL1/GEC1* (GABA[A] receptor-associated protein like 1) gene was discovered during the search for new early estrogen-induced genes in a model of guinea-pig glandular

epithelial cells.<sup>1</sup> The encoded protein is conserved throughout evolution from *C. elegans* to humans, with 100% identical protein sequence from yeast to mammals.<sup>2</sup> This protein also shares a high degree of homology with the GABARAP protein, which expresses a GABA<sub>A</sub> receptor-associated protein.<sup>3</sup> The

\*Correspondence to: Jianhua Zhang; Email: zhanja@uab.edu; Michaël Boyer-Guittaut; Email: michael.boyer-guittaut@univ-fcomte.fr  
Submitted: 01/17/2013; Revised: 02/18/2014; Accepted: 02/28/2014; Published Online: 04/01/2014  
<http://dx.doi.org/10.4161/auto.28390>

2 proteins share 87% sequence identity, a common tridimensional structure similar to the one described for ubiquitin,<sup>4</sup> and serve a similar function in GABA<sub>A</sub> receptor transport.<sup>5</sup> In addition, GEC1 was shown to interact with tubulin and promote tubulin assembly and microtubule bundling in vitro.<sup>5</sup> GEC1 was later renamed GABARAPL1. The role of GABARAPL1 in the transport of receptors is not restricted to the GABA<sub>A</sub> receptor since it interacts with human OPRK1 (opioid receptor, kappa 1) and enhances its trafficking to the plasma membrane.<sup>6</sup>

In rodents, *GABARAPL1* is highly expressed in the brain, and restricted to neurons.<sup>7-9</sup> In muscle or cardiomyocytes, it is activated after glucose deprivation, oxidative stress or ultra-endurance exercise.<sup>10,11</sup> In most tumor cell lines or cancer tissues tested, *GABARAPL1* expression is lower than noncancerous tissues or cells.<sup>12,13</sup> Inhibition of *GABARAPL1* expression has also been observed in muscles of Duchenne muscular dystrophy patients,<sup>14,15</sup> in the skeletal muscle of patients presenting an upper motor neuron lesion<sup>15</sup> or in the substantia nigra of Parkinson disease patients.<sup>16</sup> Whether the changes of *GABARAPL1* expression are contributing to the disease pathogenesis or compensatory responses to various pathological conditions is currently unclear.

Recently, we have demonstrated that GABARAPL1, like GABARAP, can associate with autophagic vesicles and is involved in the autophagy process.<sup>2</sup> The autophagy pathway is a cellular degradation pathway involved in the degradation of long-lived proteins and organelles.<sup>17-21</sup> This is in contrast to the proteasome pathway which is involved in the specific degradation of ubiquitinated short-lived proteins.<sup>22</sup> Autophagy requires more than 30 Atg8-related (ATG) proteins, and the regulated formation of a double-membrane structure known as the phagophore. Following its initiation, this structure elongates and engulfs part of the cytoplasm containing organelles, aggregates or soluble proteins, to form a closed vesicle called the autophagosome. This vesicle will later fuse with the lysosomes, to form an autolysosome, and induce the degradation of its content, a process that is involved in maintaining mitochondrial quality and in the responses to oxidative stress.<sup>23-25</sup> The initiation and the elongation of this structure requires several ATG proteins, including orthologs of yeast Atg8, which are conjugated to phospholipids of the elongating double-membrane structure via a cycle similar to the one described for the ubiquitination of proteins.<sup>22</sup> These Atg8 orthologs are divided into 2 subfamilies: the MAP1LC3 (microtubule-associated protein 1 light chain 3) family, usually abbreviated as LC3, and the GABARAP family which together comprises LC3A, B, B2 and C and GABARAP, GABARAPL1, and GABARAPL2, respectively. These proteins were initially thought to serve redundant functions in the formation of the autophagosome.

Recent studies have shown that in HeLa cells, the proteins of the LC3 family are indispensable for the elongation of the double-membrane structure while the GABARAP family members are required for the late maturation of the autophagosomes.<sup>26</sup> In the course of these experiments, siRNA directed against each of the 7 *ATG8* orthologs inhibited SQSTM1/p62 degradation. However, cross-regulation among individual siRNAs was not

examined. Out of the 7 *ATG8* family genes, *Lc3b* and *Gabarap* genes have been knocked out in mice. Mice with disruption of the *Gabarap* or the *Lc3b* gene alone are viable and without an apparent change in phenotype.<sup>27,28</sup> It is noteworthy that alterations of the autophagy pathway have not been reported with the *Gabarap* knockout mice. The fact that these animals are viable, fertile, and do not exhibit any noticeable phenotype is in favor of the redundancy theory. Recent studies, however, have shown that *Lc3b* KO mice exhibited decreased autophagic vesicles in the lung after chronic exposure to cigarette smoke, suggesting that in response to a specific stimulus, individual *ATG8* ortholog genes may play important and distinct roles in autophagy.<sup>29</sup>

Consistent with these observations, one recent hypothesis to explain the high number of Atg8 orthologs in mammals is their possible involvement in different types of selective autophagy (e.g., aggrephagy, mitophagy, pexophagy, ribophagy, or xenophagy).<sup>30</sup> Adaptor proteins, such as SQSTM1, NBR1 (neighbor of BRCA1 gene 1), and BNIP3L/NIX, interact with ubiquitinated aggregates or organelles via their ubiquitin associated domains and recruit cargos to the autophagosomes by interacting with different ATG8 members via their LC3-interacting region (W/YxxL/I). Several studies have indicated that the distinct Atg8 family members have different affinities for the specific cargos and therefore might be the missing link to explain the selectivity of the autophagy process. For example, it has been shown that all Atg8 members can bind BNIP3L in vitro but only GABARAPL1 is preferentially recruited to damaged mitochondria in a BNIP3L-dependent manner in cells treated with the mitochondrial uncoupler CCCP.<sup>31</sup> Another study showed that GABARAPL1 can specifically bind to STBD1 (starch-binding domain 1)/genethonin1 and induce glycogen degradation by autophagy in a process now known as glycophagy.<sup>32</sup> This process is also dependent on the STBD1 LC3-interacting region and seems to be specific to GABARAPL1.<sup>33</sup> A third study recently demonstrated that GABARAPL1 inhibits Wnt-CTNNB1/β-catenin signaling in MCF-7 cells via the selective degradation of DVL2 (dishevelled segment polarity protein 2), an activator of the WNT-CTNNB1 pathway.<sup>34</sup> In addition, overexpression of GABARAPL1 inhibits MCF-7 cell proliferation and the formation of tumors in nude mice.<sup>34</sup> Whether the role of GABARAPL1 in regulating cell proliferation and tumor formation is linked to the degradation of DVL2 or the autophagy pathway has not been determined. These observations suggest that different Atg8 members may be involved in selective autophagy processes linked to the degradation of specific cargos, occurring in distinct cell types or tissues or in response to different stressors.

Since GABARAPL1 is involved in glycogen degradation, relocalizes to damaged mitochondria and interacts with BNIP3L, we hypothesized that GABARAPL1 may play an essential role in cell metabolism and in particular in energy production. This function may also explain the fact that overexpression of this protein inhibits MCF-7 breast cancer cell proliferation and tumor formation.<sup>13,34</sup> Indeed, it is known that highly proliferating breast cancer cells need increased levels of ATP and that tumor formation requires an active autophagy pathway to

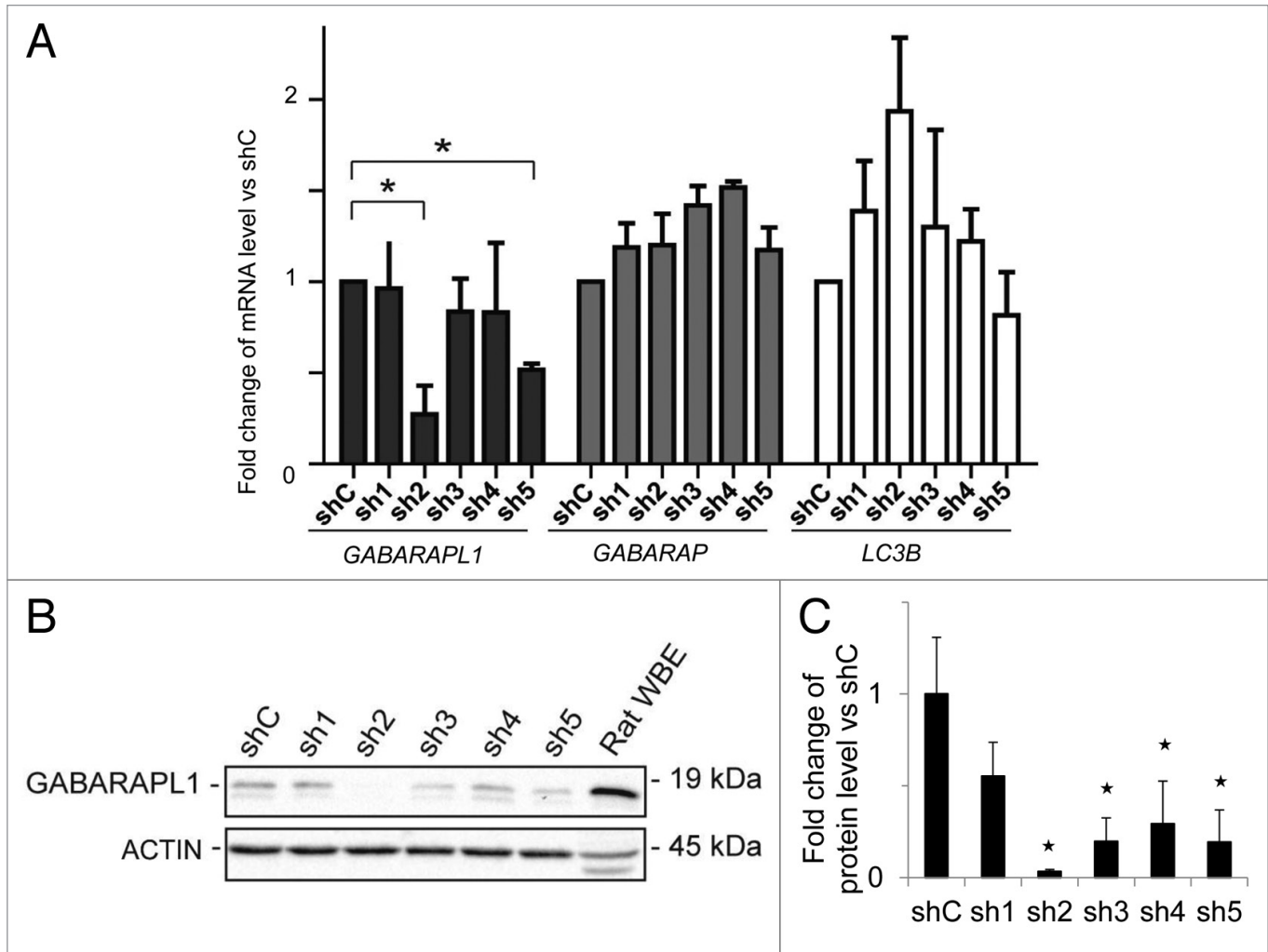


**Figure 1.** *GABARAPL1* mRNA and protein expression are significantly decreased in the MDA-MB-436-sh2 clone. (A) *GABARAPL1*, *GABARAP*, and *LC3B* mRNA expression was analyzed by qRT-PCR in the different MDA-MB-436 stable cell lines. The different stable cell lines, expressing 1 of the 5 shRNAs directed against the *GABARAPL1* gene (sh1 to sh5), were compared with the stable MDA-MB-436 cell line expressing a control shRNA (shC). \* $P < 0.05$ , vs shC (n = 3). (B) *GABARAPL1* expression levels in the MDA-MB-436 stable cell lines were determined by western blotting. Total proteins (40  $\mu$ g) were separated on a 15% SDS-PAGE gel and immunoblotted using anti-*GABARAPL1* and anti-ACTIN antibodies and the ECL Plus reagent. A representative experiment of 3 performed is shown. Rat whole brain extract (WBE) was used as a positive control of *GABARAPL1* expression. (C) Quantification of the signals observed on the western blot in (B). \* $P < 0.05$ , vs shC (n = 3).

survive under hypoxic and oxidative stress before the vascularization of a solid tumor.<sup>35</sup>

In this study, we stably expressed 5 different shRNAs targeting *GABARAPL1* in the MDA-MB-436 cell line, which is the only breast cancer cell line, to our knowledge, that has detectable levels of the protein. This protocol allowed us to select cell lines targeting only *GABARAPL1*, without affecting *GABARAP* or *LC3B*, and study the function of this knockdown on the phenotype of breast cancer cells. Our data showed that several shRNAs specific to *GABARAPL1* decreased mRNA expression but only 2 significantly decreased levels of the *GABARAPL1* protein. These stable cell lines exhibited increased cell growth, decreased autophagic flux, and decreased lysosome number. Furthermore, decreased *GABARAPL1* led to increased glutathione (GSH) and ATP, increased basal respiration as well as increased numbers of mitochondria. These observations support the hypothesis that

the lower levels of *GABARAPL1* in cancer cells inhibit autophagic flux and thereby the turnover of mitochondria leading to their accumulation and an increase of basal respiration, levels of ATP, and GSH. This increased energetic and antioxidant capacity in response to the suppression of *GABARAPL1* could then contribute to more aggressive phenotypes in cancer cells.

## Results

### Establishment of *GABARAPL1* knockdown stable cell lines

MDA-MB-436 cells were transfected with 5 different shRNA-*GABARAPL1*-expressing vectors (directed against the open reading frame of the gene) and a shRNA-control-expressing vector, and we selected 5 antibiotic-resistant clones for each shRNA. Cells with stable transfection of shRNA-*GABARAPL1*

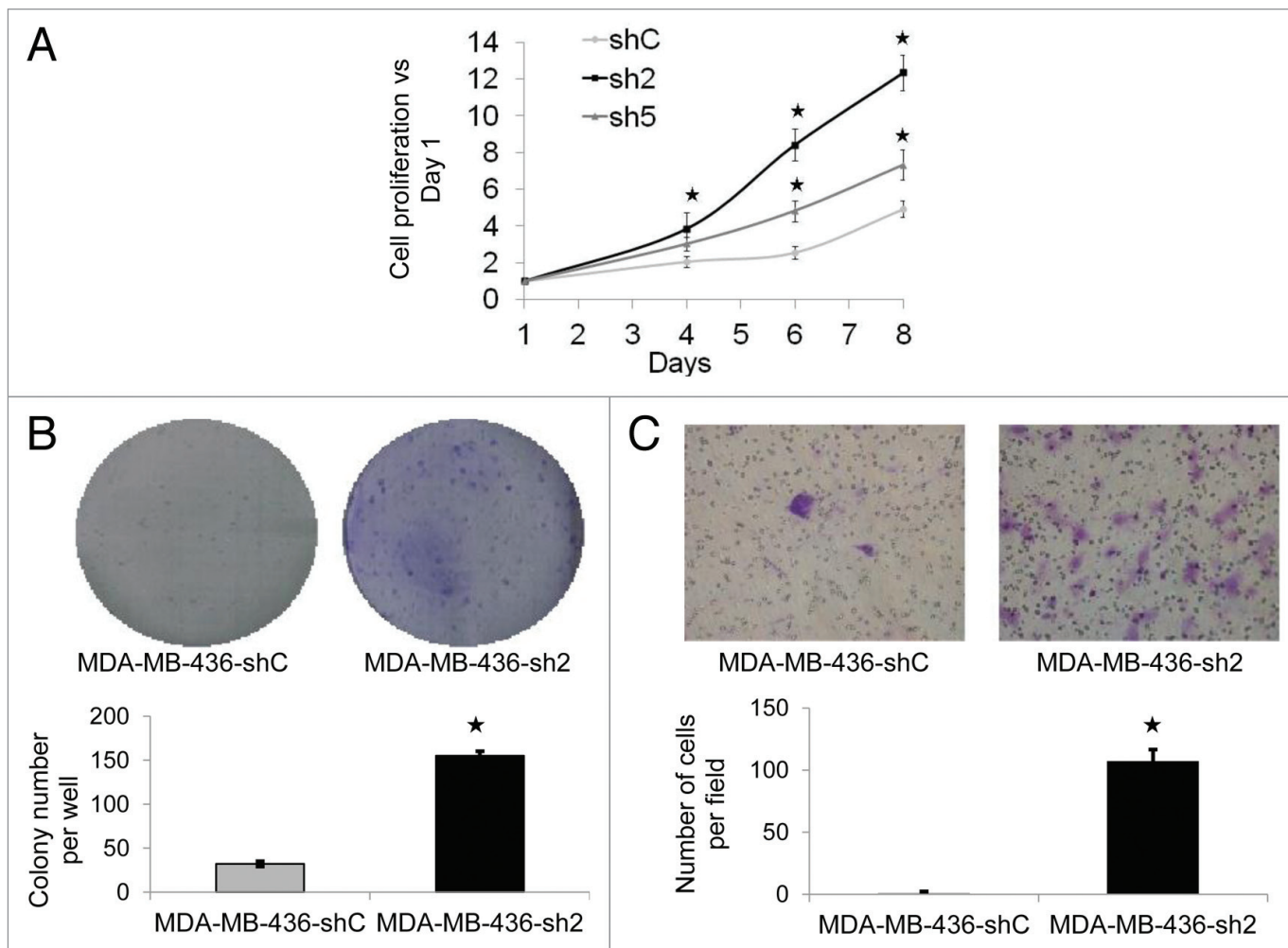


**Figure 2.** GABARAPL1 knockdown promotes cell growth, colony formation, and invasion. (A) MDA-MB-436-shC, sh2 and sh5 cell growth was determined using a MTT assay over an 8-d period. All data were normalized to the number of cells at d 1 for each cell line. \* $P < 0.05$ , vs shC (n = 24). (B) MDA-MB-436-shC and sh2 cells (3,000 in 6-well plates) were grown for a period of 12 d then fixed and stained with crystal violet. The number of colonies was then determined using the Vision-Capt software (VilberLourmat). A representative experiment of 3 performed is shown. \* $P < 0.05$ , vs shC (n = 3). (C) MDA-MB-436-shC and sh2 cells were grown in modified Boyden chambers coated with ECM gel. After a 24 h incubation at 37 °C, cells in the upper chamber were swabbed while cells in the lower chamber were fixed, stained with crystal violet and counted using a light microscope at a high magnification ( $\times 400$ ). A representative experiment of 3 performed is shown. \* $P < 0.05$ , vs shC (n = 3).

sh2 exhibited the greatest decrease in the mRNA (80%) (Fig. 1A) and protein expression (96%) levels (Fig. 1B and C) compared with the control cell line expressing the shRNA control (shC), without changing *GABARAP* and *LC3B* mRNA levels. In a second cell line, cells with stable transfection of shRNA-*GABARAPL1* sh5 exhibited a 50% decrease of *GABARAPL1* mRNA (Fig. 1A) and an 80% decrease in protein levels (Fig. 1B and C).

#### GABARAPL1 regulates MDA-MB-436 proliferation, colony formation ability, and cell invasion

We investigated whether the decrease of *GABARAPL1* expression in the MDA-MB-436 cell line would alter its tumor cell-linked features such as proliferation, colony formation, and invasion. We first performed an MTT assay over an 8-d period to determine whether *GABARAPL1* regulated cell proliferation. We observed that the sh2 and sh5 cell lines exhibited

an increased proliferation rate compared with the shC control cell line (Fig. 2A). We also confirmed that this increase was not due to a decrease in cell death (data not shown). That the sh5 cell line exhibited a lower increase in proliferation compared with the sh2 cells is consistent with the observation that *GABARAPL1* is decreased by 80% in sh5 compared with 96% in sh2 cells (Fig. 1C). We then assessed the ability of the sh2 cell line to form new colonies. As shown in Figure 2B, after 14 d, we found a significantly higher number of colonies formed with the sh2 cell line compared with the shC cell line. Furthermore, using a modified Boyden chamber, we found that the sh2 cells exhibited a substantially higher capacity for migration (Fig. 2C). We have also tested the ability of the sh5 cells to form new colonies and migrate in a Boyden chamber but did not detect any significant change compared with the control cells (Data not shown). This can be explained by the

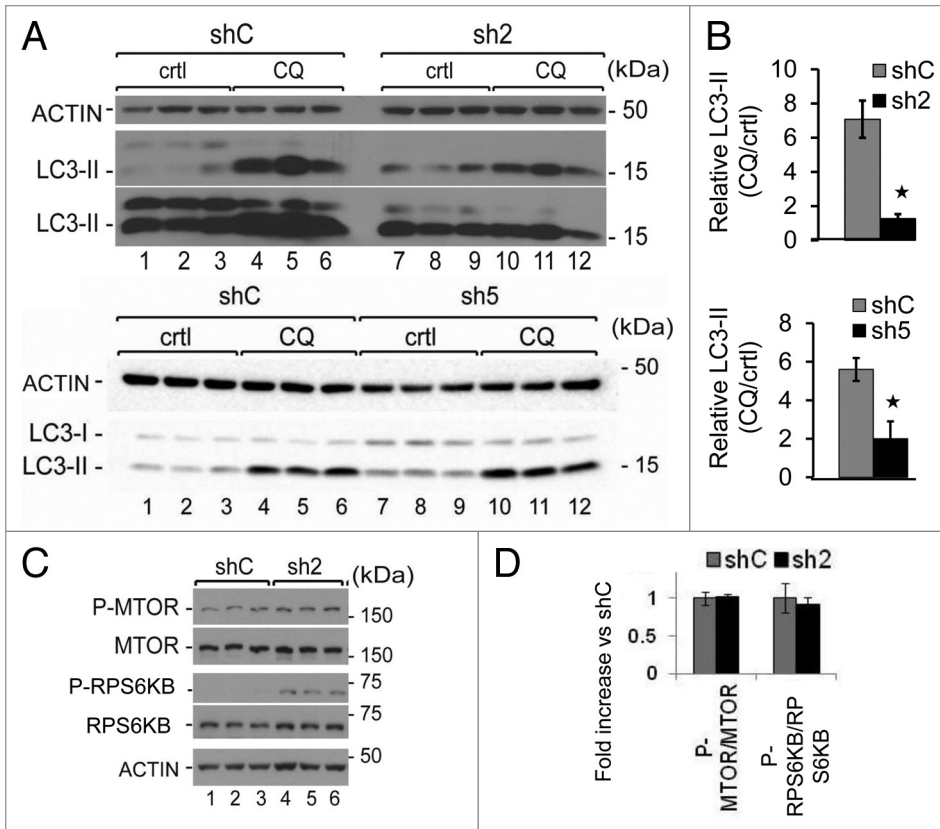


**Figure 3.** GABARAPL1 knockdown inhibits autophagic flux without changing MTOR signaling. (A) MDA-MB436-shC, sh2, and sh5 cells were cultured for 5 h in the presence (lanes 4 to 6 and 10 to 12) or absence (lanes 1 to 3 and 7 to 9) of the lysosome inhibitor chloroquine (40  $\mu$ M). Total proteins (25  $\mu$ g) were separated on 12% SDS-PAGE gels followed by immunoblotting with anti-LC3 and anti-ACTIN antibodies and the ECL Plus reagent. A representative experiment of 3 performed is shown. (B) The autophagic flux was determined as the levels of LC3-II in the presence of chloroquine divided by the levels of LC3-II in absence of chloroquine. \* $P < 0.05$ , vs shC ( $n = 3$ ). (C) MDA-MB436-shC and sh2 cells were cultured for 24 h at 37  $^{\circ}$ C and 5%  $\text{CO}_2$  then total proteins (25  $\mu$ g) were separated on 12% SDS-PAGE gels followed by immunoblotting with anti-phospho-MTOR, anti-MTOR, anti-phospho-RPS6KB, anti-RPS6KB, and anti-ACTIN antibodies and the ECL Plus reagent. A representative experiment of 3 performed is shown. \* $P < 0.05$ , vs shC ( $n = 3$ ). (D) Quantification of the signals observed on the western blot in (C) ( $n = 3$ ).

fact that the decrease of *GABARAPL1* in the sh5 cells is less than that observed in the sh2 cells.

#### GABARAPL1 knockdown inhibits autophagic flux

We have previously shown that GABARAPL1 associates with autophagosomes.<sup>2</sup> To investigate whether loss of GABARAPL1 alters autophagic flux, we quantified the levels of LC3-II, the autophagosome-associated form of the protein, in the absence and presence of the lysosomal inhibitor chloroquine, in the 3 cell lines, shC, sh2 and sh5. We found that the basal levels of LC3-II were not significantly changed by suppressing the levels of GABARAPL1 in sh2 but were increased in sh5 cells (Fig. 3A, comparing lanes 1 to 3 and 7 to 9,  $P < 0.05$  comparing LC3-II/ACTIN between shC and sh5 cells). We calculated the ratio between the LC3-II levels with and without chloroquine as an index of overall autophagic flux,<sup>36</sup> and observed a decrease of this ratio in the sh2 and sh5 cell lines compared with the control cells (Fig. 3B). These data indicate that a loss of GABARAPL1 results in a decrease in autophagic flux. To

determine whether this attenuation of autophagic flux was due to an inhibition of autophagy induction or the degradation of autophagosomes, we first examined MTOR activation. We found that MTOR and RPS6KB/p70S6K phosphorylation levels were similar in the shC and sh2 cell lines (Fig. 3C and D). Moreover, both shC and sh2 cells increase autophagic flux in response to rapamycin, a MTOR-dependent inducer, as indicated by an increase of LC3-II levels (Fig. S1A–S1C). Autophagic flux as defined by the ratio LC3-II in response to rapamycin+CQ/LC3-II in response to rapamycin is similar in shC and sh2 cells (Fig. S1D). However the flux in the presence of rapamycin and in the absence of rapamycin is similar in shC cells, and significantly increased in sh2 cells (Fig. 3B, which is also included in Fig. S1D for direct comparison). In contrast, sh2 cells exhibited a greater increase in LC3-II in response to trehalose, a MTOR-independent autophagy inducer, compared with shC cells, and no further increase in LC3-II when both trehalose and chloroquine were present (Fig. S2A–S2C). Hence, the sh2 cell line exhibited a lower increase of autophagic flux in response to trehalose compared with shC cells (Fig. S2D). These data suggest that GABARAPL1 knockdown does not change MTOR signaling, but changes the autophagic response to rapamycin.

Both rapamycin and trehalose inhibited sh2 cell proliferation (Fig. S3A and S3B). As shown in Figure S1 and Figure S2, autophagic flux was increased in sh2 cells in response to rapamycin, whereas it was unchanged in response to trehalose. Therefore, the inhibition of proliferation by rapamycin or trehalose cannot be simply attributed to an increase in autophagic flux. Consistent with this interpretation, we found no change in cell proliferation for sh2 cells following transfection of *ATG7* or nontargeting siRNA (Fig. S3C and S3D), despite a significant knockdown of *ATG7*, suggesting that further inhibition of autophagy in sh2 cells does not affect proliferation.

#### GABARAPL1 knockdown increases *SQSTM1* mRNA, *SQSTM1* protein, as well as *BECN1* protein levels

Since we did not detect any change in MTOR signaling associated with GABARAPL1 knockdown, we examined the levels of other key proteins in the autophagic-lysosome pathway and found an increase of *BECN1*/Beclin 1 and *SQSTM1* protein levels in the sh2 and sh5 cells

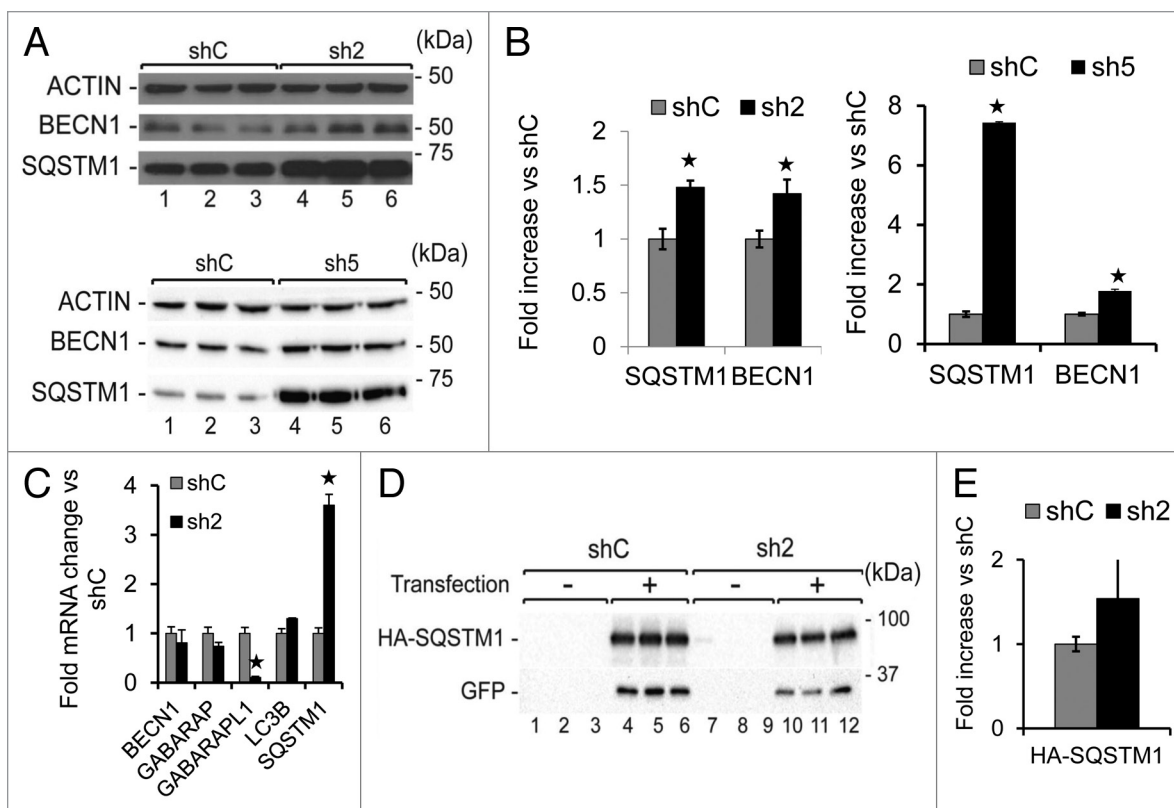


**Figure 4.** GABARAPL1 knockdown leads to increased SQSTM1 and BECN1 proteins. (A) MDA-MB436-shC, sh2, and sh5 cells were cultured for 24 h at 37 °C and 5% CO<sub>2</sub> then total proteins (25 µg) were separated on 12% SDS-PAGE gels followed by immunoblotting with anti-BECN1, anti-SQSTM1, and anti-ACTIN antibodies and the ECL Plus reagent. A representative experiment of 3 performed is shown. (B) Quantification of the signals observed on the western blot in (A). \**P* < 0.05, vs shC (n = 3). (C) *GABARAPL1*, *GABARAP*, *LC3B*, *BECN1*, and *SQSTM1* mRNA expression was analyzed by qRT-PCR in the MDA-MB436-shC and sh2 cells. \**P* < 0.05, vs shC (n = 3). (D) MDA-MB436-shC and sh2 cells were cotransfected with the vectors expressing HA-SQSTM1 and pEGFP-N1 (ratio 10:1). Forty-eight hours after transfection, total proteins (25 µg) were separated on 12% SDS-PAGE gels, followed by immunoblotting with anti-HA, anti-GFP, and anti-ACTIN antibodies and the ECL Plus reagent. A representative experiment of 3 performed is shown. (E) Quantification of the signals observed on the western blot in (D). \**P* < 0.05, vs shC (n = 3).

(Fig. 4A and B). Since the transcription of genes encoding these proteins may change according to the stress status of the cells,<sup>37</sup> we performed quantitative real-time RT-PCR, and found a significant increase in *SQSTM1* (about 4-fold) but not *BECN1* mRNA levels (Fig. 4C). Therefore, increased transcription of *SQSTM1* in response to the loss of *GABARAPL1* may have contributed to the changes in its protein levels. Nevertheless, the loss of *GABARAPL1* also attenuated autophagic flux. To determine whether *SQSTM1* protein also accumulates in sh2 cells independent of transcription, we transfected shC and sh2 cells with a pCMV-HA-SQSTM1 construct, in which *SQSTM1* expression is under the control of a constitutive CMV promoter. Our data showed a 50% increase in HA-SQSTM1 levels in the sh2 cells compared with the shC cells (Fig. 4D and E). These results suggest that both an increase of transcription and a decrease of autophagic flux contribute to the higher levels of *SQSTM1* in sh2 cells.

#### GABARAPL1 knockdown decreases *LAMP1* mRNA and protein levels

Next we examined lysosome protein levels in shC, sh2, and sh5 cells. We found a significant decrease of *LAMP1* (by 50%) in sh2 cells but not sh5 cells (Fig. 5A and B). The decreased

*LAMP1* protein in sh2 cells may be due to decreased transcription as *LAMP1* mRNA levels were also decreased by 30% in sh2 cells (Fig. 5C). Interestingly, both sh2 and sh5 cells exhibited significant decrease of *LAMP1* immunostaining compared with shC cells (Fig. 5D). This discrepancy between *LAMP1* western blot analyses and *LAMP1* immunostaining may be due to a difference in protein denaturation procedure in western blotting and in immunostaining. Intriguingly, a decrease of *LAMP1* protein level is not associated with a decrease of lysosomal protease activities. We found that lysosomal CTSB (cathepsin B) activity and protein levels are unchanged, whereas CTSD (cathepsin D) activity and protein levels are increased, in sh2 cells compared with shC cells (Fig. S4A–S4C). This increase of CTSD may be a compensatory response to a decrease of *LAMP1*, as prior studies report that a decrease in lysosome number leads to the induction of cathepsin activities.<sup>38,39</sup>

#### GABARAPL1 knockdown increases mitochondrial membrane potential and the demand for mitochondrial bioenergetics

To determine the effects of *GABARAPL1* on mitochondrial membrane potential we used TMRM staining and found a significant increase in the sh2 cells compared with shC cells, and that it decreased to the same levels by FCCP as expected

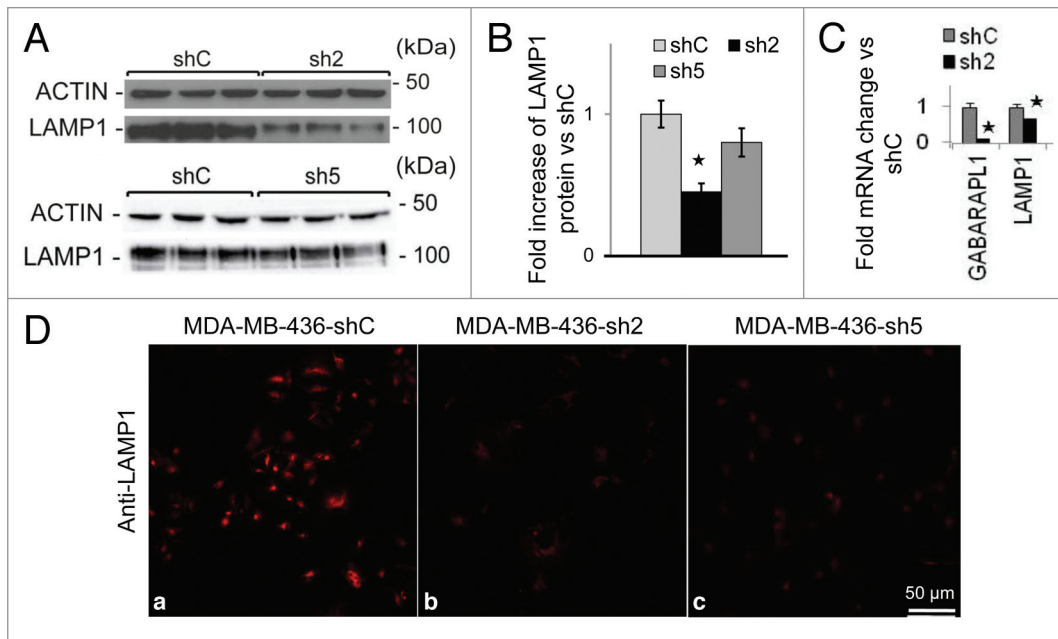


**Figure 5.** GABARAPL1 knockdown leads to decreased LAMP1 protein levels and immunocytochemistry staining. (A) MDA-MB436-shC, sh2, and sh5 cells were cultured for 24 h at 37 °C and 5% CO<sub>2</sub> then total proteins (25 μg) were separated on 12% SDS-PAGE gels followed by immunoblotting with anti-LAMP1 antibodies and the ECL Plus reagent. A representative experiment of 3 performed is shown. (B) Quantification of the signals observed on the western blot in (A). \**P* < 0.05, vs shC (n = 3). (C) *GABARAPL1* and *LAMP1* mRNA expression was analyzed by qRT-PCR in the MDA-MB436-shC and sh2 cells. \**P* < 0.05, vs shC. (D) MDA-MB436-shC, sh2 and sh5 cells were cultured for 24 h at 37 °C and 5% CO<sub>2</sub>, fixed, permeabilized, blocked with 5% BSA, incubated with a monoclonal anti-mouse LAMP1 overnight at 4 °C and then with an Alexa Fluor 555 goat anti-mouse for 1 h. The cells were then analyzed using a confocal microscope. Each picture is representative of a typical cell staining observed in 10 fields chosen at random.

(Fig. 6A). In addition, MitoTracker Red staining (Fig. 6B) was also increased in the sh2 cell line, consistent with either an increase in mitochondrial membrane potential or mitochondrial number. Similarly, MitoTracker Red intensity is higher in both sh2 and sh5 cells compared with shC cells as assessed by confocal microscopy (Fig. 6C and D).

We then used the Seahorse XF24 analyzer to determine whether GABARAPL1 knockdown changed mitochondrial function.<sup>24,40</sup> The shC and sh2 cells were plated at similar confluency (Fig. 7A). We then monitored the basal levels of oxygen consumption rate (OCR), and OCR following injection of oligomycin, an inhibitor of ATP synthase, FCCP, an uncoupler, and antimycin A, an inhibitor of mitochondrial complex III (Fig. 7B). We were then able to calculate basal, ATP-linked, proton leak (non-ATP linked), maximal, reserve capacity, and nonmitochondrial OCR (Fig. 7C).<sup>24,40,41</sup> We found an increase in basal OCR in sh2 cells, which was largely due to an increase in non-ATP linked proton leak respiration, consistent with a higher membrane potential. We also determined the extracellular acidification rate (ECAR), which can be ascribed to glycolysis and other proton-generating processes in the cells, but did not detect differences between the 2 cell lines (Fig. 7D). Furthermore, we did not observe any changes of maximal OCR or reserve capacity (Fig. 7C), nor the state apparent (Fig. 7E), in response to GABARAPL1 knockdown, however, the RCR basal and maximal were decreased in sh2 cells compared with shC cells (Fig. 7E). Interestingly, we found that GABARAPL1-suppressed cells had higher amounts

of ATP compared with the control cells, which suggests that the mitochondrial population in these cells is capable of meeting the increased demands for proliferation through increased metabolic activity (Fig. 7F).

#### GABARAPL1 knockdown leads to an increase of mitochondrial protein levels and an increase of damaged mitochondrial DNA

An altered autophagy-lysosome pathway may result in an increased mitochondrial number in GABARAPL1 knockdown cells. Therefore, we then examined whether the levels of proteins involved in mitochondrial biogenesis or homeostasis would be altered in sh2 cells. We found that levels of both PPARGC1A, which is involved in mitochondria biogenesis,<sup>42</sup> and VDAC1, which is involved in the flux of metabolites to and from the mitochondria,<sup>43</sup> were upregulated in sh2 cells compared with shC cells (Fig. 8A and B). Levels of MFN1 (mitofusin 1), which is involved in mitochondria fusion,<sup>44</sup> DNMI1/Drp1 (dynamin 1-like), which is involved in mitochondria fission,<sup>45</sup> PINK1 and PARK2/PARKIN, which are involved in mitophagy,<sup>46</sup> were unchanged. Our data support the hypothesis that GABARAPL1 is important in maintaining mitochondrial homeostasis by promoting autophagic flux, independent of mitochondrial fission/fusion or selective mitophagy.

As an additional index of mitochondrial number we measured mtDNA copy number relative to the genomic DNA. As shown in Figure 8C, we found increased levels of mtDNA in sh2 cells compared with shC cells. These data also suggest that both an attenuation of autophagic flux and an increase in mitochondrial

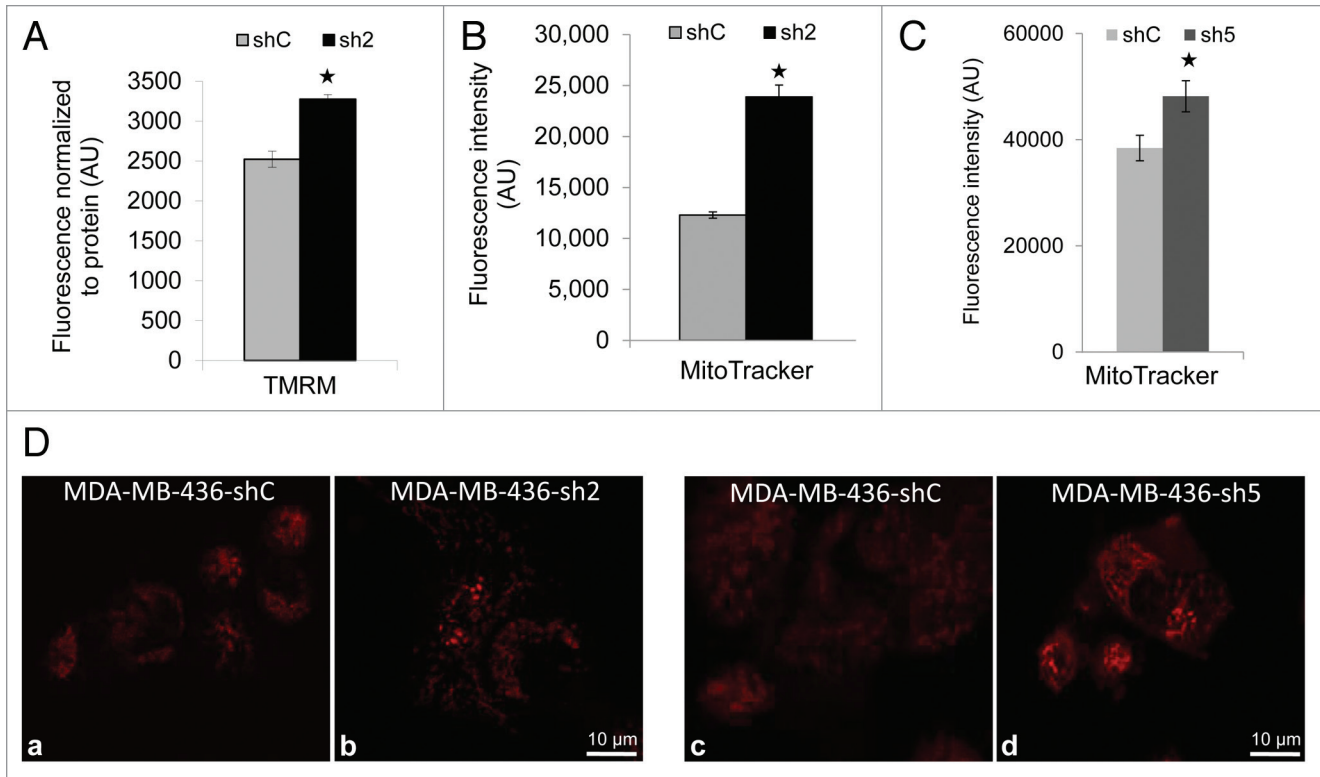


**Figure 6.** GABARAPL1 knockdown increases TMRM and MitoTracker Red staining. **(A)** TMRM staining (AU, arbitrary units) normalized to total protein. MDA-MB436-shC and sh2 cells (40,000) were cultured in 96-well plates for 24 h at 37 °C and 5% CO<sub>2</sub>. Cells were then incubated with 100 nM TMRM for 45 min before being washed with PBS. TMRM fluorescence was measured at 590 nm using a Victor<sup>3</sup>V PerkinElmer Wallace 1420 Multilabel Counter. FCCP as a control decreased mitochondrial membrane potential to ~750 in both shC and sh2 cells. \**P* < 0.05, vs shC (n = 3). **(B)** MitoTracker Red fluorescence values (AU) for the 2 cell lines shC and sh2. Cells (600,000) were cultured in 6-well plates for 24 h at 37 °C and 5% CO<sub>2</sub>, stained with 50 nM MitoTracker Red for 45 min at 37 °C, trypsinized, washed with PBS and resuspended in 500  $\mu$ l PBS. Intracellular fluorescence was then assessed using the LSR-II Becton Dickinson flow cytometer. \**P* < 0.05, vs shC (n = 3). **(C)** MDA-MB436-shC and sh5 cells (100,000) were cultured in Labtek 4-well plates for 24 h at 37 °C and 5% CO<sub>2</sub>, stained with 50 nM MitoTracker Red for 45 min at 37 °C and washed with PBS. Mitochondria were imaged using the Zeiss LSM 710 confocal microscope and the Zen 2008 software. MitoTracker intensity was quantified by Image J for 25 cells for each cell line in 5 different fields of view chosen at random. \**P* < 0.05, vs shC. **(D)** MDA-MB436-shC and sh2 cells (100,000) were cultured in Labtek 4-well plates for 24 h at 37 °C and 5% CO<sub>2</sub>, stained with 50 nM MitoTracker Red for 45 min at 37 °C and washed with PBS. Similarly, MDA-MB436-shC and sh5 cells (100,000) were cultured, stained with MitoTracker Red, and imaged. The pictures were taken with the Zeiss LSM 710 confocal microscope.

biogenesis via PPARGC1A increase<sup>42</sup> may contribute to an increased MitoTracker staining, mtDNA copy number, mitochondrial membrane potential, and VDAC1 protein levels. To further assess mitochondrial health, we measured mtDNA damage, and found that sh2 cells exhibited significantly higher mtDNA damage compared with shC cells (Fig. 8D). mtDNA copy number is increased in sh5 cells compared with shC but mtDNA damage in sh5 is comparable to shC, this may reflect an incomplete GABARAPL1 knockdown in sh5 cells (data not shown).

The accumulation of mitochondria and the changes of mitochondrial quality suggest a defect in mitochondrial clearance in sh2 cells. To quantify mitochondrial clearance, we have performed costaining of mitochondria and lysosomes in the presence or absence of FCCP (Fig. S5). We found a slight increase of MitoTracker Red and LysoTracker Green colocalization in sh2 cells compared with shC cells; this may be due to an increase of mitochondrial number, and is not consistent with an attenuated selective mitophagy. We did not find a significant difference of

FCCP-induced colocalization of mitochondria and lysosomes in shC or sh2 cells. Similarly, we did not find colocalization of GFP-PARK2 with mitochondria in shC or sh2 cells (data not shown) but it is conceivable that the potential defects in mitochondrial clearance in sh2 cells are independent of PARK2 translocation to the mitochondria. The exact mechanism of how accumulation of underperforming mitochondria occurs in sh2 cells remains unclear.

#### GABARAPL1 knockdown promoted cell survival in response to HNE

We incubated shC and sh2 cells with increasing concentrations of HNE, a product of lipid peroxidation previously described to decrease mitochondrial activity,<sup>40,41,47</sup> through its modification of proteins including ATP5B (ATP synthase, H<sup>+</sup> transporting, mitochondrial F1 complex,  $\beta$  polypeptide)<sup>48</sup> or SIRT3.<sup>49</sup> As shown in Figure 9A, after 16 h, the viability of sh2 cells was higher than shC cells after incubation with different concentrations of HNE, indicating that GABARAPL1 knockdown enhances cell survival in response to HNE.



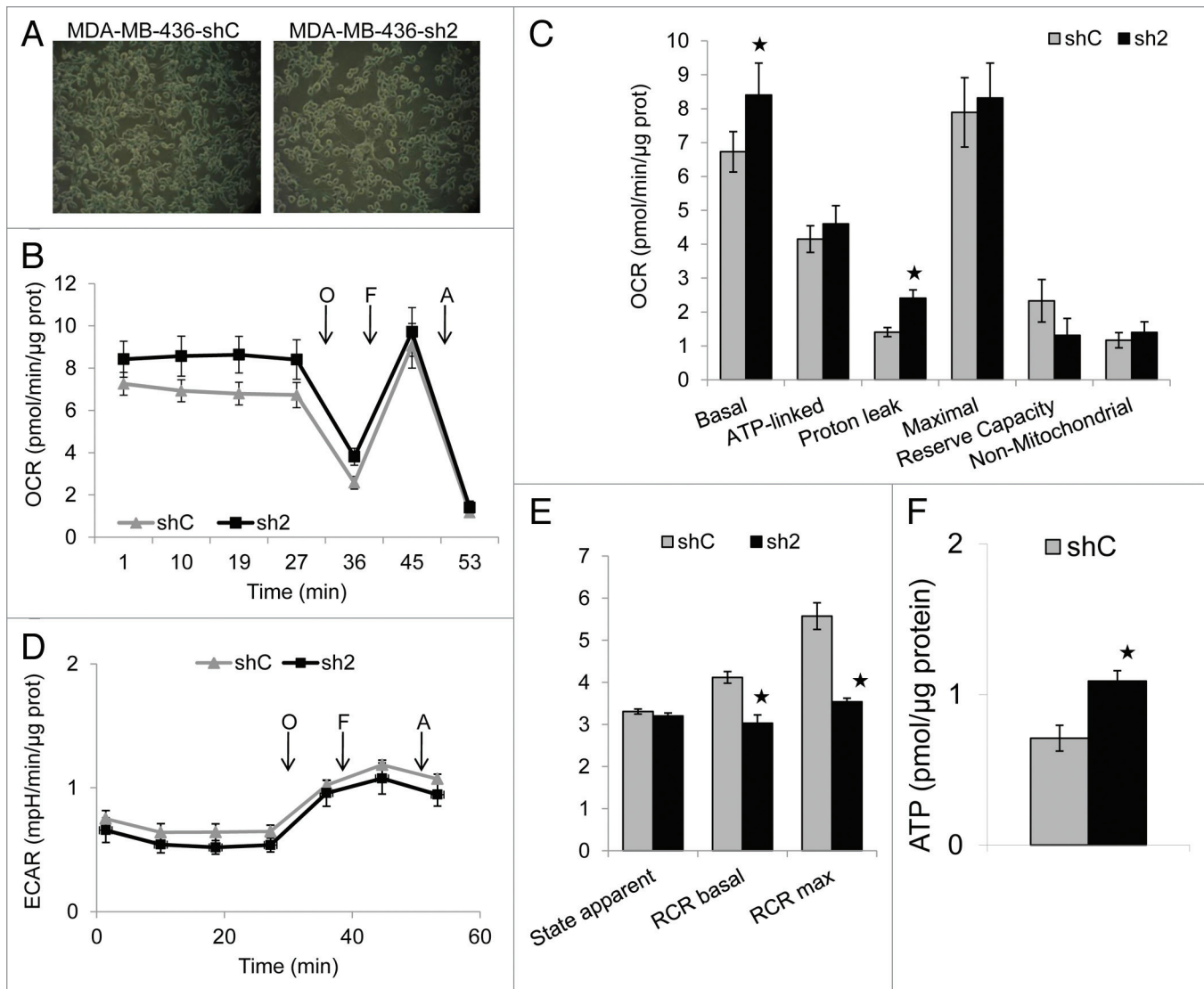


**Figure 7.** GABARAPL1 knockdown increases basal and proton-leak oxygen consumption rate (OCR), increases intracellular ATP levels, and decreases basal and maximal respiratory control ratio (RCR). MDA-MB436-shC and sh2 cells (60,000) were cultured for 24 h in 24-well XF24 Seahorse Biosciences V7 microplates and then bioenergetic function was assessed using the Seahorse XF24 analyzer. Both OCR and ECAR were measured. The ATP synthase inhibitor oligomycin (O; 1  $\mu$ M), uncoupler FCCP (F; 0.75  $\mu$ M), and complex III inhibitor antimycin A (A; 10  $\mu$ M) were injected at the indicated times to determine different parameters of mitochondrial function. (A) Pictures showing similar confluency of the shC and sh2 cells before the start of the Seahorse analysis. (B) OCR values shown as pmol  $O_2$ /min/ $\mu$ g protein. (C) Histogram showing the comparison of basal, ATP-linked, proton leak-linked, maximal, and non-mitochondrial OCR of shC and sh2 cells. Nonmitochondrial OCR was determined as the OCR after antimycin A treatment. Basal OCR was determined as OCR before oligomycin minus OCR after antimycin A. ATP-linked OCR was determined as OCR before oligomycin minus OCR after oligomycin. Proton leak was determined as basal OCR minus ATP-linked OCR. Maximal OCR was determined as the OCR after FCCP minus nonmitochondrial OCR. Reserve capacity was defined as the difference between maximal OCR after FCCP minus basal OCR. \* $P < 0.05$ , vs shC (n = 4). (D) Extracellular acidification rate (ECAR) values were plotted as mpH/min/ $\mu$ g protein for shC and sh2 cells (n = 4). (E) Histogram showing the comparison of state apparent, RCR basal and RCR maximal of shC and sh2 cells. State apparent was determined as the value corresponding to the following formula:  $4 - [(Basal - Oligo)/(Basal - FCCP)]$ . RCR basal was determined as the value corresponding to the following formula:  $(Basal - AntiA)/(Oligo - AntiA)$ . RCR maximal was determined as the value corresponding to the following formula:  $(FCCP - AntiA)/(Oligo - AntiA)$ . \* $P < 0.05$ , vs shC (n = 4). (F) Histogram showing intracellular ATP values (pmoles/ $\mu$ g protein) for shC and sh2 cells. MDA-MB436-shC and sh2 cells (40,000) were cultured in 96-well plates for 24 h at 37  $^{\circ}$ C and 5%  $CO_2$ . The intracellular ATP concentration was then determined using the ATPlite kit from PerkinElmer according to the manufacturer's instructions. Luminescence was measured using a Victor<sup>2</sup>V PerkinElmer Wallace 1420 Multilabel Counter. \* $P < 0.05$ , vs shC (n = 3).

To determine effects of HNE on autophagic flux in sh2 cells, we assessed the LC3-II levels (Fig. 9B and C). We found that LC3-II levels were significantly increased in the shC cells (-1.4-fold) but unchanged in sh2 cells following HNE exposure. Consequently, the ratio of LC3-II with HNE vs. LC3-II without

HNE was also lower in the sh2 cells. Basal HNE-protein adducts were higher in sh2 cells compared with shC cells (Fig. 9D and E) (compare lanes 1 to 3 and 4 to 6). After exposure to exogenous HNE, HNE-protein adduct levels increased to 1.5-fold in the shC cells but did not change in the sh2 cells (Fig. 9D

and E). Next we determined the levels of GSH in the 2 cell lines, since the formation of HNE-protein adducts could be attenuated by intracellular cellular glutathione (GSH) which can detoxify HNE through the action of glutathione transferases.<sup>50</sup> As shown in Figure 9F, GSH levels were significantly higher in the sh2 cell lines, suggesting that the decreased HNE-induced cell death in sh2 cells may be partially provided by the higher levels of GSH.

## Discussion

Recent studies have shown that GABARAPL1 is associated with autophagic vesicles<sup>2</sup> and the *GABARAPL1* gene may be a tumor-suppressor gene and a prognostic biomarker in breast cancer.<sup>13</sup> GABARAP, the closest homolog of GABARAPL1, is expressed at low levels in invasive ductal and invasive lobular carcinomas compared with normal breast tissue, and the overexpression of GABARAP in CAL51 decreases their proliferation rate as well as their ability to form colonies in soft-agar and to form tumors in nude mice.<sup>51</sup> GABARAPL1 overexpression has been shown to inhibit proliferation of the breast cancer cell line (MCF-7),<sup>13</sup> and their ability to form tumors in nude mice.<sup>34</sup> Building on these data, we hypothesized that endogenous GABARAPL1 plays a role in suppressing the cancer cell phenotype and in mediating autophagy. In this study, we established stable cell lines that exhibited significant loss of *GABARAPL1* mRNA and protein levels (Fig. 1), and found that these cells exhibited an increased proliferation rate, colony formation and invasion (Fig. 2) consistent with the hypothesis that *GABARAPL1* is a tumor suppressor gene.

Autophagy plays a complex role in tumor initiation and progression. On the one hand, autophagy protects against the production of reactive oxygen species in the cells and their deleterious effects in mutating DNA and promoting cell transformation.<sup>35</sup> On the other hand, autophagy is required for the transformation of mouse embryonic fibroblasts by the Ras oncogene and this effect is linked to its role in nutrient recycling such as glucose uptake and increased glycolytic flux.<sup>52</sup> During the later stages of in vivo tumor formation, autophagy has been shown to be necessary for the cancer cell survival in hypoxia before the vascularization of the tumor.<sup>35</sup> Autophagy has also been shown to protect against cellular stress induced by the chemotherapeutic drugs used in cancer treatment leading to several clinical trials involving the use of an inhibitor of the autophagy flux as a combination therapy.<sup>53</sup> Even though the mechanism is still unclear, many studies suggest a role of autophagy in the regulation of cancer cell metabolism allowing them to meet the requirements for rapid proliferation. Using multiple autophagic flux analyses, including comparing LC3-II levels with and without chloroquine, endogenous *SQSTM1* mRNA and protein levels, as well as exogenous

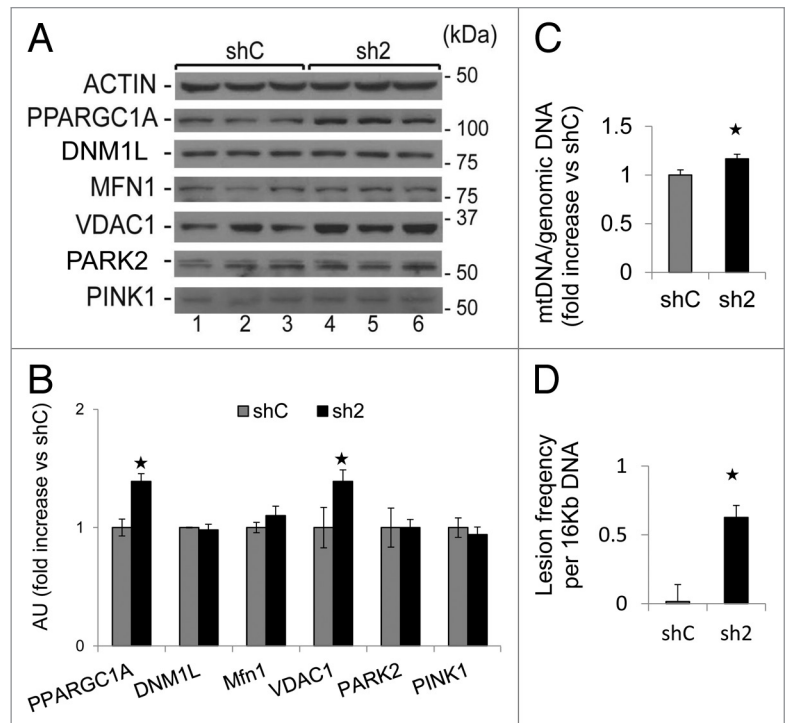


**Figure 8.** GABARAPL1 knockdown increases mitochondria number, and mtDNA damage. (A) MDA-MB436-shC and sh2 cells were cultured for 24 h at 37 °C and 5% CO<sub>2</sub>. Cells were then lysed in the presence of protease and phosphatase inhibitors and total proteins (25 μg) were separated on 12% SDS-PAGE gels followed by immunoblotting with anti-PPARGC1A, anti-DNMM1L, anti-MFN1, anti-VDACC1, anti-PARK2, anti-PINK1, and anti-ACTIN antibodies and the ECL Plus reagent. A representative experiment of 3 performed is shown. (B) Quantification of the signals on the western blot in (A). \**P* < 0.05, vs shC (n = 3). (C) MDA-MB436-shC and sh2 cells (600,000) were cultured in 6-well plates for 24 h at 37 °C and 5% CO<sub>2</sub>. Cells were washed with PBS and kept frozen at -80 °C until purification of total DNA. Specific genomic and mitochondrial DNA sequences were amplified by quantitative real-time PCR. The data are presented as the ratio of mitochondrial vs. genomic DNA and normalized to the control cell line, shC. \**P* < 0.05, vs shC (n = 3). (D) MDA-MB436-shC and sh2 cells (600,000) were cultured in 6-well plates for 24 h at 37 °C and 5% CO<sub>2</sub>. Cells were washed with PBS and kept frozen at -80 °C until purification of total DNA. Specific long and short mitochondrial DNA sequences were amplified by PCR. The data were calculated from the levels of long mitochondrial PCR product vs. levels of short mitochondrial PCR product as described in Materials and Methods, and normalized to shC. \**P* < 0.05, vs shC (n = 3).

constitutively expressed pCMV-HA-SQSTM1 (Fig. 3A and B; Fig. 4D and E), we have found that GABARAPL1 knockdown cells exhibit a decreased autophagic flux. Interestingly, sh5 cells with incomplete GABARAPL1 knockdown also exhibited decreased autophagic flux, although to a less extent than sh2 cells and did not result in the same colony formation and migration phenotypes as the sh2 cells.

The underlying mechanism of attenuated autophagic flux as a result of GABARAPL1 knockdown appears to be a significant decrease of LAMP1 protein levels and lysosome number (Fig. 5A–D), supporting the hypothesis that loss of GABARAPL1 leads to an attenuation of autophagosomal degradation. Importantly, we did not find a difference in the phosphorylation of MTOR and RPS6KB between control and GABARAPL1 knockdown cells, suggesting an

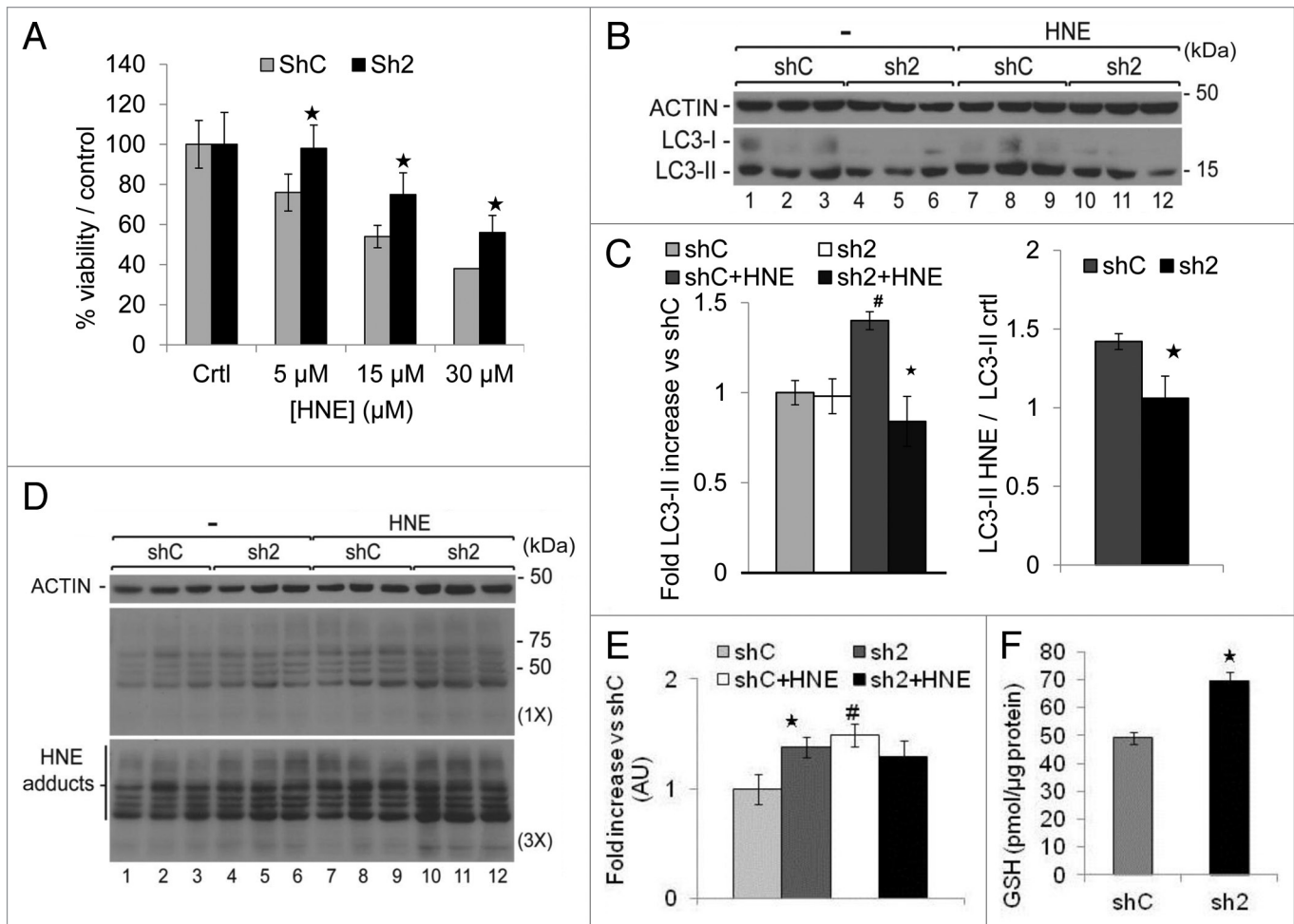


**Figure 9.** GABARAP1 knockdown enhances cell survival in response to HNE, inhibits autophagic flux in response to HNE, and increases intracellular HNE-protein adducts and glutathione (GSH) concentration. **(A)** MDA-MB436-shC and sh2 cells were grown for 16 h in the presence of HNE (0, 5, 15 or 30 µM). Cells were then trypsinized and counted in the presence of trypan blue. The values were normalized to the number of cells determined in the control samples for each cell line. \* $P < 0.05$ , vs shC (n = 3). **(B)** MDA-MB436-shC and sh2 cells were cultured for 16 h in the presence of HNE (30 µM). Cells were then lysed and total proteins (25 µg) were separated on 12% SDS-PAGE gels followed by immunoblotting with anti-LC3 and anti-ACTIN antibodies and the ECL Plus reagent. A representative experiment of 3 performed is shown. **(C)** Quantification of the LC3-II signals observed in the western blots shown in **(B)**. HNE-induced changes of LC3-II levels were determined as the levels of LC3-II in response to HNE divided by the levels of LC3-II without HNE. \* $P < 0.05$ , vs shC (n = 3), # $P < 0.05$ , vs untreated cells (n = 3). **(D)** MDA-MB436-shC and sh2 cells were cultured for 16 h in the presence of HNE (30 µM). Cells were then lysed in HNE lysis buffer containing 10 mM N-ethylmaleimide and total proteins (25 µg) were separated on 12% SDS-PAGE gels followed by immunoblotting with anti-4-HNE and anti-ACTIN antibodies and the ECL Plus reagent. **(E)** Quantification of the signals observed in the western blot in **(D)**. \* $P < 0.05$ , vs shC (n = 3), # $P < 0.05$ , vs untreated cells (n = 3). **(F)** Total cellular GSH was determined using the GSH recycling assay, as described in Materials and Methods, using a Beckman Coulter DU-800 spectrophotometer, after shC and sh2 cells (600,000) were cultured in 6-well plates for 24 h at 37 °C. \* $P < 0.05$ , vs shC (n = 3).

MTOR-independent attenuation of autophagic flux (Fig. 3C and D). Furthermore, we found increased BECN1 levels that cannot explain an attenuation of autophagic flux (Fig. 4A–C). Previous studies have shown that autophagy and lysosomal genes are coordinately regulated by master transcription activators and repressors,<sup>54–56</sup> such coordinate regulation appears to be perturbed in GABARAP1 knockdown cells. In this context, it has been previously shown that rapamycin and trehalose are able to induce TFEB (transcription factor EB), a transcription factor specifically inducing the transcription of genes involved in the autophagosomal and lysosomal biogenesis including LAMP1.<sup>54,55</sup> We found that rapamycin and trehalose inhibited cell

proliferation and abolished the effects of GABARAP1 suppression on cell proliferation. The effects of rapamycin and trehalose on cell proliferation may be linked to an increase in LAMP1. Furthermore, although the exact mechanisms are unclear, our observation that LAMP1 is decreased and CTSD is increased in sh2 cells is consistent with prior findings and supports a differential role of lysosomal components in cell proliferation.<sup>57–59</sup>

GABARAP1 has been previously linked to the selective autophagy of mitochondria, shown to interact with BNIP3L, a mitochondrial protein, and to be recruited to mitochondria to induce their clearance during the maturation of reticulocytes.<sup>31</sup> Because mitophagy degrades damaged mitochondria

and therefore suppresses reactive oxygen species formation and DNA damage, and that our results showed that autophagic flux is attenuated in the absence of GABARAPL1, we determined whether GABARAPL1 knockdown would lead to desensitization to mitochondrial stressor-induced autophagy. Indeed, we found that in response to HNE, which is a byproduct of lipid peroxidation previously shown to modify mitochondrial proteins and inhibit their activity,<sup>24,41,48</sup> GABARAPL1 knockdown cells exhibit less of an increase in LC3-II levels compared with control shC cells (Fig. 9B and C). However, cell survival in response to HNE is dependent on GABARAPL1 (Fig. 9A). Further, GABARAPL1 knockdown induced a higher level of total endogenous HNE-protein adducts in the cells, and there were no further increases after additional HNE exposure in these cells (Fig. 9D). Additionally, glutathione steady-state levels are increased in the GABARAPL1 knockdown cells compared with control cells (Fig. 9G), and the higher level of glutathione may form conjugates with the exogenously added HNE to inhibit its toxic effect in the cells.<sup>60</sup> The increase of endogenous HNE-protein adducts may be due to the attenuation of autophagic flux, and the increased adducts may also signal to induce an antioxidant response for the cells to produce more enzymes involved in glutathione synthesis.<sup>61</sup>

We also determined the impact of GABARAPL1 knockdown on mitochondrial function. We found that GABARAPL1 knockdown cells exhibited increased mitochondrial membrane potential, mitochondrial biogenesis factor PPARGC1A, mitochondrial protein VDAC1, both total and damaged mtDNA (Figs. 6–8). In addition to exhibiting decreased autophagic flux as discussed above (Fig. 4), sh5 cells with incomplete GABARAPL1 knockdown also exhibited increased total mtDNA but not damaged mtDNA (Fig. 8), suggesting that autophagic flux and accumulation of mitochondrial mass are sensitive to moderate change of GABARAPL1 levels, whereas increased colony formation, cell migration/invasion, and mtDNA damage occur only when GABARAPL1 level decreases more than 70% (Fig. 1).

These competing impacts on mitochondrial homeostasis due to *GABARAPL1* knockdown resulted in a cellular bioenergetic profile that did not substantially deviate from that of the control shC cells, other than a significant increase in proton leak (Fig. 7). Importantly, ATP levels were increased in response to GABARAPL1 inhibition showing that although a decrease in mitochondrial quality occurred, the overall mitochondrial population was still competent to meet the energetic demands of the cell. This could be due to the activation of mitochondrial biogenesis in attempt to restore the integrity of the mitochondrial population and a small but active population of functioning mitochondria.

Our study supports the model that GABARAPL1 inhibition induces a depletion of LAMP1 and lysosomal number, attenuates autophagic flux, and leads to an accumulation of damaged mitochondria, associated with stimulated mitochondrial biogenesis leading to increased mitochondrial number, mitochondrial protein, mitochondrial membrane potential, mitochondrial respiration, and ATP levels (Fig. 10). The increase of mitochondrial number and cellular glutathione, which itself could be stimulated

by an increase in the basal levels of mitochondrial reactive oxygen species, further resulted in resistance to cell death, and may contribute to increased proliferation and aggressiveness of these cells. Our data demonstrate that GABARAPL1 plays an important role in regulating the autophagy-lysosome pathway, mitochondrial activity, cell metabolism, and proliferation.

## Materials and Methods

### Reagents and antibodies

Cell culture reagents were purchased from Invitrogen. The following antibodies were used: polyclonal anti-GABARAPL1 (Proteintech, 11010-1-AP, 1:1,000), polyclonal anti-LC3B (Sigma-Aldrich, L8918, 1:3,000), monoclonal anti-SQSTM1/p62 (Abnova, H00008878-M01, 1:3,000), monoclonal anti-LAMP1 (Developmental hybrid studies, H4a3, 1:1000), monoclonal anti-VDAC1 (Abcam, ab16816, 1:1000), monoclonal anti-DNM1L/Drp1 (Abcam, ab56788, 1:1000), polyclonal anti-MFN1 (Santa Cruz, H65 sc-50330, 1:1000), polyclonal anti-PPARGC1A (Santa Cruz, H300 sc-13067, 1:1000), monoclonal anti-PINK1 (Abcam, ab23707, 1:1000), polyclonal anti-PARK2 (Santa Cruz, H300 sc-30130, 1:1000), goat anti-4-HNE (Alpha diagnostics, HNE12-S, 1:3000), polyclonal rabbit anti-MTOR (Cell Signaling, 2983, 1:1000), polyclonal rabbit anti-phospho-MTOR (Cell Signaling, 2971, 1:1000), polyclonal rabbit anti-RPS6KB (Cell Signaling, 9202, 1:1000), polyclonal rabbit anti-phospho-RPS6KB (Cell signaling, 9205, 1:1000), polyclonal rabbit anti-CTSB (Santa Cruz, sc-13985, 1:1000), polyclonal goat anti-CTSD (Santa Cruz, sc-6486, 1:1000), and polyclonal anti-ACTIN (Sigma-Aldrich, A5060, 1:10,000). Bafilomycin A<sub>1</sub> (Sigma, B1793) was prepared as a 50  $\mu$ M stock in DMSO. Rapamycin (Sigma-Aldrich, R8781) was purchased as a 2.74 mM stock in DMSO. Chloroquine (Sigma-Aldrich, C6628) was prepared as a 200 mM stock in water. Tetramethylrhodamine methyl ester perchlorate (TMRM, Sigma-Aldrich, T5428) was prepared as a 100 mM stock in DMSO. 3-Methyladenine (3-MA, Sigma-Aldrich, M9281) was prepared fresh as a 10 mM working solution in complete culture medium. Oligomycin (O4876), FCCP (C2920) and antimycin A (A8674) were purchased from Sigma-Aldrich. 4-hydroxynonenal (HNE) was prepared fresh from a stock solution purchased from Calbiochem (393204). The HA-SQSTM1-expressing vector was purchased from Addgene (28027, Dr Qing Zhong).

### Cell culture and stable cell lines

The MDA-MB-436 cell line (ATCC) was maintained in DMEM medium (Dulbecco's modified Eagle's medium; Invitrogen, 11965-092) containing 1 mM L-glutamine and supplemented with 10% fetal bovine serum (Atlanta Biologicals, S111-50), 100  $\mu$ g/ml penicillin/streptomycin (Invitrogen, 15140-122) and 1 mM sodium pyruvate (Invitrogen, 11360-070) in a 5% CO<sub>2</sub> incubator at 37 °C. Cells were split every 4 d (1:3 dilution). The MDA-MB-436-shRNA-*control* (shC or control) and -*GABARAPL1* (sh2 or GABARAPL1 KD) cell lines were maintained in complete medium supplemented with 1  $\mu$ g/ml puromycin (Invitrogen, 28-111-QL). To create these stable

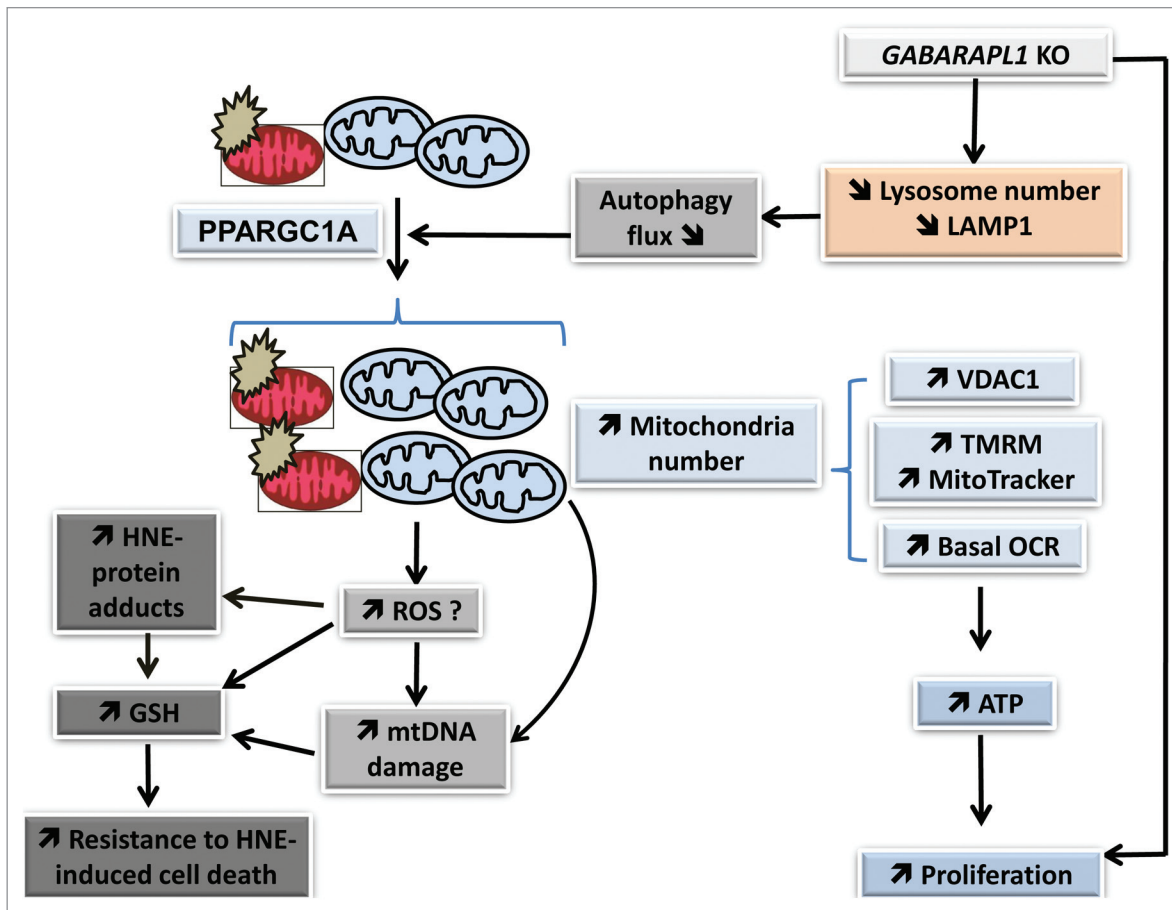


**Figure 10.** GABARAPL1 function in breast cancer cells. Our studies indicate that GABARAPL1 plays an important role in autophagic flux, mitochondrial homeostasis, metabolic programming, and control of cell proliferation in breast cancer MDA-MB-436 cells. *GABARAPL1* knockdown induces a disruption of the autophagosome-lysosome pathway leading to a decrease of lysosome number and accumulation of damaged mitochondria, increased mitochondrial biogenesis and number, and increased mitochondrial respiration, mitochondrial membrane potential, mitochondrial proteins, and mtDNA damage. This is further evidenced by an increase of HNE-protein adducts, increased antioxidant response, and increased ATP levels. The increase of mitochondrial number, cellular glutathione, and cellular ATP may contribute to resistance to cell death and increased proliferation.

cell lines, MDA-MB-436 cells ( $10^6$ ) plated in 10-cm diameter cultures dishes were transfected the day after plating using 10  $\mu$ g of 5 different pKo.1-puro-shRNA-*GABARAPL1* vectors (Mission shRNA, Sigma-Aldrich, SHCLNG-NM\_031412, shRNA 443s1c1) and 1 pKo.1-puro-shRNA-control vector (Sigma-Aldrich, SHC002) and 20  $\mu$ l TransFast reagent (Promega, E2431) according to the manufacturer's protocol. After 48 h incubation, 3  $\mu$ g/ml puromycin was added to each plate and the medium was changed every 2 d for the next 14 d until the appearance of antibiotic-resistant single clones. Five resistant clones for each shRNA transfection were then tested for the expression of *GABARAPL1*, *GABARAP*, and *LC3B* mRNAs and proteins by qRT-PCR and western-blotting, respectively. The stable cell lines used later on in this study are the MDA-MB-436-shRNA-control clone 2 (shC or control) and the MDA-MB-436-shRNA-*GABARAPL1* clone 2 (sh2 or *GABARAPL1* KD). The sh5 clone has been designed using the same protocol as described for the sh2 clone but using a different shRNA (Mission shRNA, Sigma-Aldrich, SHCLNG-NM\_031412, shRNA 570s1c1).

#### Quantitative real-time RT-PCR analysis

Total RNAs were extracted using the TRI Reagent (Invitrogen, AM9738). To remove any genomic DNA contamination, total RNAs were treated with RNase-free DNase I (Invitrogen, AM2222) and purified with phenol/chloroform. A volume of 1  $\mu$ g of total RNAs was reverse transcribed using M-MLV RT (Sigma-Aldrich, M1302) and oligo(dT)15 primers following the manufacturer's instructions. Quantitative PCR was run on the Step One Real Time PCR System (Applied Biosystems) using the SYBER Green PCR Master Mix (Applied Biosystems, 4309155) and the following parameters: 10 min at 95  $^{\circ}$ C followed by 40 cycles: 15 s at 95  $^{\circ}$ C and 1 min at 60  $^{\circ}$ C. The target genes levels (*GABARAPL1*, *GABARAP*, *LC3B*, *LAMP1*, *SQSTM1*, and *BECN1*) were normalized to the levels of the *H3B2* housekeeping gene (forward: 5'-GCTAGCTGGA TGCTCTTTTGG G-3' and reverse: 5'-GTGGTAAAGC ACCCAGGAAA-3'). The primer sequences were: *GABARAPL1* (5' CCCTCCCTTG GTTATGATCC A-3' and 5'-AGGAAGGGAT TGCTGGGTTC T-3'), *GABARAP* (5'-ACTCCCACCC CACAAAATCC-3' and 5'-GCCTTTCCCA

TCCTGCTGTA-3'), *LC3B* (5'-CGGAAAGCAG CAGTGTACCA-3' and 5'-GGCAGAAGGG AGTGTGTCTG A-3'), *LAMP1* (5'-GTGTCTGCTG GACGAGAACA-3' and 5'-ATGAGGACGA TGAGGACCAG-3'), *SQSTM1* (5'-AAATGGGTCC ACCAGGAAAC TGGA-3' and 5'-TCA ACT TCAA TGCCCAGAGG GCTA-3') and *BECN1* (5'-TCACCATCCA GGAACTCACA-3' and 5'-CCTGGCGAG GAGTTTCAAT A-3'). Each sample was analyzed in triplicate and then differences in the expression of each gene were quantified using the  $\Delta\Delta C_t$  approach using the endogenous control.

#### Western blot analysis

Cells were lysed in RIPA lysis buffer (50 mM TRIS-HCl pH 7.8, 150 mM NaCl, 2 mM EDTA, 1% Triton X-100, 0.1% SDS supplemented with protease inhibitors [Sigma, P8340]) then 25 or 50  $\mu$ g of lysates were resolved on a 12% or 15% polyacrylamide gel in running buffer (25 mM Tris base, 192 mM glycine, 0.1% SDS) at 60 V for 60 min and 120 V for another 60 min. Proteins were transferred onto Immuno-Blot PVDF 0.2  $\mu$ m membranes (Bio-Rad, 162-0177) for 90 min at 90 V at 4 °C in transfer buffer (25 mM Tris base, 192 mM glycine, 0.037% SDS, 20% methanol). Membranes were subsequently incubated in blocking buffer for 1 h (TBS-T [20 mM TRIS-HCl, pH 7.6, 137 mM NaCl, 0.1% Tween 20] containing 5% skim milk powder) and incubated with primary antibodies in blocking buffer overnight at 4 °C. The secondary horseradish peroxidase-coupled anti-rabbit (Sigma-Aldrich, A0545) and anti-mouse IgG antibodies (Sigma-Aldrich, A4416) were prepared in TBS-T. After 1 h incubation, the membrane was washed 3 times in TBS-T and incubated with the Pierce ECL western blotting substrate (Pierce, 32106) according to the manufacturer's recommendations. All western blots were analyzed using the ChemiDoc XRS+ from Bio-Rad. All western blot signals were quantified before saturation using the Image Lab 2.0 software provided with the ChemiDoc XRS+ according to the manufacturer's instructions.

For the HNE western-blotting, cells were lysed in HNE lysis buffer (50 mM HEPES, 150 mM NaCl, 1.5 mM MgCl<sub>2</sub>, 1 mM EDTA, 1% glycerol, 1% NP40 [Fisher Scientific, NC9375914]) supplemented with protease inhibitors (Sigma-Aldrich, P8340) and 50 mM N-ethylmaleimide (Sigma-Aldrich, E3876). The samples were run the same day to avoid any freeze-thaw step. The goat anti-HNE antibody was purchased from Alpha Diagnostics (HNE-12S) and used at a 1:3000 dilution overnight in TBS-T supplemented with 5% horse serum (Life Tech Corp, 16050-130).

#### Cell proliferation assays

For the MTT assay, MDA-MB-436-shC and MDA-MB-436-sh2 cell lines were plated in 96-well plates (3,000 cells per well, 24 wells per cell line) and MTT assays were conducted every day over a 10-d period using 3-(4,5-dimethylthiazol-2-yl)-2,5-diphenyl tetrazolium bromide (MTT) (Sigma-Aldrich, M5655) as previously described.<sup>13</sup>

For the trypan blue exclusion assay, MDA-MB-436-shC and MDA-MB-436-sh2 cells were plated in 12-well plates (100,000 cells per well, 3 wells per cell line) and cells were counted every

day over a 4 d period. After discarding the culture medium, cells were incubated in 100  $\mu$ l Trypsin-EDTA (Invitrogen, 25200-056) for 5 min at 37 °C. After further addition of 200  $\mu$ l of complete medium, cells were supplemented with 30  $\mu$ l of trypan blue (0.04% final concentration, Cellgro, 25-900-CI) and the viable cells density was then determined using a Malassez hemocytometer.

#### Colony formation assay

MDA-MB-436-shC and MDA-MB-436-sh2 cells were plated in 6-well plates (3,000 cells per well) and incubated in complete culture medium supplemented with 10% fetal bovine serum, 100  $\mu$ g/mL penicillin/streptomycin and 1 mM L-glutamine at 37 °C and 5% CO<sub>2</sub>. After 12 d, the colonies formed were fixed 10 min with 100% ethanol and stained for 10 min with crystal violet (0.5% in 2% ethanol). Each well was then washed 3 times with distilled water and colonies were counted using the Vision-Capt software (VilberLourmat).

#### Cell invasion assay

Cell invasion was evaluated using modified Boyden chambers (6.5-mm diameter and 8- $\mu$ m pore size, SPL Life Sciences, 35224). Boyden chambers were coated with 50  $\mu$ g ECM gel from Engelbreth-Holm-Swarm murine sarcoma (Sigma-Aldrich, E1270) diluted in DMEM and incubated for 5 h at 37 °C. 100,000 cells in 250  $\mu$ l of serum-free DMEM were seeded into the upper chamber and 500  $\mu$ l of complete culture medium were added in the lower compartment. After 24 h incubation in a 5% CO<sub>2</sub> incubator at 37 °C, cells on the upper surface were removed using a swab and cells on the lower surface were fixed 5 min with absolute ethanol and stained with crystal violet (0.5% in 2% ethanol) for 10 min. The filters were then washed with distilled water and cells were counted using a light microscope at a high magnification ( $\times 400$ ).

#### CTSB and CTSD activity assays

CTSB and CTSD activities were quantified using the CTSB Activity Assay Kit (Abnova, KA0766) and the CTSD activity assay kit (Sigma, CS0800) following manufacturer's instructions. Briefly, cells were collected by scraping and centrifugation (1500 g for 5 min at 4 °C), washed once with PBS (0.17 M NaCl, 3.3 mM KCl, 10 mM Na<sub>2</sub>HPO<sub>4</sub>, 1.8 mM KH<sub>2</sub>PO<sub>4</sub>) before a second spin and then lysed using CTSB cell lysis buffer (kit) or MES lysis buffer for CTSD (20 mM MES, pH 6.8, 20 mM NaCl, 1 mM MgCl<sub>2</sub>, 2 mM EDTA, 10 mM NaH<sub>2</sub>PO<sub>4</sub>) supplemented with phosphatase (Sigma, P0044) and protease (Sigma, P8340) inhibitors. Lysates were then incubated for 30 min on ice, centrifuged at 15000 g for 5 min and supernatants were subjected to DC-Bradford assay (Bio-Rad, 500-0114).

For the CTSB activity assay, 50  $\mu$ g of cell lysate were combined with the CTSB reaction buffer (kit) in a 96-well black plate with clear top and bottom. E64 (Sigma, E8640) was used for inhibition of CTSB activity. After addition of a fluorogenic CTSB substrate (kit), the plate was incubated for 2 h at 37 °C before values were read in fluorescence units, which were then normalized to controls.

For the CTSD activity assay, 30  $\mu$ g of lysate per sample were used for activity readings with and without pepstatin A (PepA, 2 mg/ml, Sigma, P5318) in a black 96-well plate with clear top

and bottom. PepA values were subtracted from non-PepA values to determine CTSD activity in fluorescence units, which were then normalized to control samples.

#### **Mitochondrial bioenergetic measurements using the Seahorse XF-24 analyzer**

To measure mitochondrial function in MDA-MB-436-shC and MDA-MB-436-sh2 cells, an XF24 extracellular flux analyzer (Seahorse Bioscience, North Billerica, MA, USA) was used. To allow comparison between experiments, data are expressed as the OCR in pmol/min or the extracellular acidification rate in mpH/min, normalized to cell protein contents determined by the DC-Bradford (Bio-Rad, 500-0114) method. The optimal seeding density of the cells needed to obtain measurable OCR and ECAR was established, and both ECAR and OCR show a proportional response with cell number (data not shown). For our experiments, a seeding density of 60,000 cells per well was selected to allow both increase and inhibition of OCR and ECAR. In our experiments, oligomycin, FCCP, and antimycin A concentrations were 1, 0.75, and 10  $\mu$ M, respectively.

#### **ATP assay**

MDA-MB-436-shC and MDA-MB-436-sh2 cells were plated in 96-well plates (40,000 per well) and incubated for 24 h at 37 °C. The intracellular ATP concentration was then assessed using the ATPlite kit from PerkinElmer (6016943) according to the manufacturer's recommendations. Briefly, culture medium was discarded and cells were incubated first for 5 min in the kit lysis buffer, then for further 5 min with the substrate solution, before being adapted to the dark for 10 min. Emitted luminescence was then measured using a Victor<sup>2</sup>V 1420 Multilabel Counter (PerkinElmer Wallac, Waltham, MA, USA). The intracellular ATP amounts (in pmol) were calculated according to an ATP standard curve and normalized to the quantity of protein in each sample using a DC-Bradford assay (Bio-Rad, 500-0114).

#### **GSH recycling assay**

The quantification of GSH in our 2 cell lines was performed according to the protocol previously described.<sup>62</sup> Briefly, MDA-MB-436-shC and MDA-MB-436-sh2 cells were plated in 6-well plates (600,000 per well) and incubated for 24 h at 37 °C. Culture medium was discarded and cells were washed twice in GSH wash buffer (10  $\mu$ M DTPA, diethylenetriaminepentaacetic acid, in 1 X PBS, Sigma-Aldrich, D6518) before lysis in GSH wash buffer supplemented with 0.1% Triton X-100 for 10 min on ice. Collected cells were centrifuged at 12,000 g for 15 min and supernatants were collected for GSH quantification. The reaction sample was composed of 10  $\mu$ l sample, 60  $\mu$ l DTNB [5,5'-dithiobis(2-nitrobenzoic acid), 10 mM, Sigma-Aldrich, D8130], 900  $\mu$ l GSH wash buffer, 20  $\mu$ l NAD(P)H (10 mM, Sigma-Aldrich, N1630) and 10  $\mu$ l glutathione reductase (Sigma-Aldrich, G9297). The fluorescence was then measured at 412 nm and 37 °C over a 4 min period using a DU-800 spectrophotometer (Beckman Coulter, Indianapolis, IN, USA) and the rates of the reactions were expressed in dAbs/min. The GSH amounts (in pmol) were determined according to a GSH standard curve and normalized to the quantity of protein in each sample using a DC-Bradford assay (Bio-Rad, 500-0114).

#### **TMRM staining**

MDA-MB-436-shC and MDA-MB-436-sh2 cells were plated in 96-well plates (40,000 per well) and incubated for 24 h at 37 °C. Cells were then incubated with TMRM (TetraMethylRhodamine Methyl ester perchlorate, 100 nM) in phenol-free complete medium for 45 min at 37 °C before being washed twice with PBS. TMRM fluorescence was then measured at 590 nm using a Victor<sup>3</sup>V PerkinElmer Wallac 1420 Multilabel Counter. The TMRM cell incorporation determined as arbitrary units of fluorescence was then normalized to the quantity of protein in each sample using a DC-Bradford assay (Bio-Rad, 500-0114).

#### **mtDNA quantification**

DNA was extracted from MDA-MB-436-shC and MDA-MB-436-sh2 cells. Quantitative real-time PCR was performed by using a SYBR Green master mix (Life Tech Corp, 4368708) in an ABI 7500 ((3175 Staley Road, Grand Island, NY 14072, USA). The primer sequences used for mtDNA were mtDNA-F (5'-CACCCAAGAA CAGGGTTTGT-3') and mtDNA-R (5'-TGGCCATGGG TATGTTGTTA A-3'). The primer sequences for the nuclear DNA were 18S-F (5'-TAGAGGGACA AGTGGCGTTC-3') and 18S-R (5'-CGCTGAGCCA GTCAGTGT-3') and targeted the human nuclear 18S DNA. Cycling conditions were as follows: 94 °C for 15 s, followed by 40 cycles at 94 °C for 15 s, 60 °C for 1 min and 60 °C for 1 min. The mtDNA copy number was normalized to the amplification of the 18S nuclear amplicon.

#### **mtDNA damage assay**

Mitochondrial DNA damage was evaluated by PCR method as described previously.<sup>63</sup> Briefly, total DNA was extracted and used as PCR sample. The primer sequences used for mtDNA long segment (16 kb) were mtLongF (5'-TGAGGCCAAA TATCATCTG AGGGGC-3') and mtLongR (5'-TTTCATCATG CGGAGATGTT GGATGG-3'). The primer sequences for mtDNA short (80 bp) segment were mtShortF (5'-ACCCAAGAAC AGGGTTTGT-3') and mtShortR (5'-TGGCCATGGG TATGTTGTTA A-3'). The mtDNA long and short segments were amplified using AccuPrime™ Taq DNA Polymerase High Fidelity kit (Life Tech Corp, 12346-086) and separated by agarose gel electrophoresis. The long PCR conditions were as follow: 94 °C for 11 s, followed by 27 cycles of denaturation at 94 °C for 15 s, 67 °C for 12 min and a final extension at 72 °C for 10 min. The short PCR conditions were as follow: 94 °C for 5 s, followed by 19 cycles at 94 °C for 25 s, 60 °C for 45 s, 72 °C for 1 min, and a final extension at 72 °C for 10 min. The gels were stained with ethidium bromide and visualized with AlphaImager (Cell Biosciences, Inc., Santa Clara, CA, USA). Densitometry analysis was performed using Image J software. Lesion frequency per 16 kb of mtDNA was calculated using as described previously.<sup>64,65</sup>

#### **Mitochondria staining**

Cells were plated in 4-well Labtek chambers (Nunc, 155-383) at a concentration of 100,000 cells per well and incubated at 37 °C overnight. Cells were stained in fresh complete medium with 50 nM MitoTracker® RedCMXRos (Invitrogen, M7512). Living cells were then examined using a fluorescence laser

scanning LSM 710 confocal microscope (Zeiss, Oberkochen, Germany) (UAB microscopy core, Birmingham, AL). Images were captured using the Zen 2008 software. All figures were assembled using Adobe Photoshop CS2 and Adobe Illustrator CS software.

#### LAMP1 immunostaining

Cells cultured for 24 h on coverslips in 24-well plates were washed with PBS and fixed with 4% paraformaldehyde in PBS for 15 min at room temperature. Cells were then permeabilized with 0.2% TritonX-100 in PBS for 5 min, washed 3 times for 5 min with PBS, blocked with 5% BSA (Sigma-Aldrich, A6793) in PBS for 30 min, incubated with a monoclonal anti-mouse LAMP1 (Abcam, Ab25630, 1:100) overnight at 4 °C and finally with an Alexa Fluor 555 goat anti-mouse (Life technologies, A-21422, 1:800) for 1 h. After being washed 3 times for 5 min, the cells were analyzed using a confocal microscope.

#### Mitophagy analysis

Cells (280,000) were plated in Lab-TekTMII chambers (Nunc, 155380) for 24 h and incubated at 37 °C overnight. Cells were stained in fresh complete medium with 50 nM MitoTracker® RedCMXRos (Invitrogen, M7512) and 100 nM LysoTracker® Green (Invitrogen, L-7526) for 45 min in the presence or absence of 10 μM FCCP (Sigma, C2920) for 45 min. Live cells were then analyzed using a Zeiss LSM 710 confocal microscope and the Zen 2008 software. All figures were assembled using Adobe Photoshop CS2 and Adobe Illustrator CS softwares. For mitophagy measurements, red and green pixel intensity overlay was conducted using ImageJ software (Coloc 2) and the Pearson's coefficient.

#### Flow cytometry

Cells were plated in 6-well plates at a concentration of 600,000 cells per well and incubated at 37 °C overnight. Cells were stained in fresh complete medium with 50 nM MitoTracker® RedCMXRos for 45 min. After 2 PBS washes, cells were trypsinized and resuspended in 200 μl complete medium before

being harvested at 5,000 g for 5 min and resuspended in 500 μl PBS. Cells (10,000 events) were then examined using a LSR II Becton Dickinson flow cytometer (UAB Flow Cytometry Core, Birmingham, AL). Data were acquired and analyzed using the Becton Dickinson FACScan Flow Cytometer software.

#### Statistical analyses

Statistical analyses were performed using the Student *t* test. Data are expressed as the mean ± SEM.

#### Disclosure of Potential Conflicts of Interest

VDU is a member of the Seahorse Biosciences Scientific Advisory Board.

#### Acknowledgment

Michaël Boyer-Guittaut would like to thank his colleagues from the EA3922 team, Jacques Bahi, president of the Université of Franche-Comté, Abderrazzak Kadmiri, director of UFR-ST of the Université of Franche-Comté and the Université of Franche-Comté for their support during this research project performed at the University of Alabama in Birmingham, AL, USA. Laura Poillet is supported by a fellowship of the Région de Franche-Comté. The authors acknowledge funding from the following sources: Dr Jianhua Zhang was supported by NIH R01-NS064090 and a VA merit award. Flow cytometry was supported by RDCC-APCC core (NIH P30 grant #P30 AR48311). The authors would like to thank Enid F Keyser (UAB Flow cytometry core, Birmingham, AL) for her technical help using the LSR-II Becton Dickinson flow cytometer. Authors are grateful to Jianhua Zhang's and Victor M Darley-Usmar's laboratory members for their technical help, advice, and critical reviewing of this manuscript.

#### Supplemental Materials

Supplemental materials may be found here: [www.landesbioscience.com/journals/autophagy/article/28390](http://www.landesbioscience.com/journals/autophagy/article/28390)

#### References

1. Pellerin I, Vuillermoz C, Jouvenot M, Ordener C, Royez M, Adessi GL. Identification and characterization of an early estrogen-regulated RNA in cultured guinea-pig endometrial cells. *Mol Cell Endocrinol* 1993; 90:R17-21; PMID:8495796; [http://dx.doi.org/10.1016/0303-7207\(93\)90161-C](http://dx.doi.org/10.1016/0303-7207(93)90161-C)
2. Chakrama FZ, Seguin-Py S, Le Grand JN, Fraichard A, Delage-Mourroux R, Despouy G, Perez V, Jouvenot M, Boyer-Guittaut M. GABARAPL1 (GEC1) associates with autophagic vesicles. *Autophagy* 2010; 6:495-505; PMID:20404487; <http://dx.doi.org/10.4161/auto.6.4.11819>
3. Wang H, Bedford FK, Brandon NJ, Moss SJ, Olsen RW. GABA(A)-receptor-associated protein links GABA(A) receptors and the cytoskeleton. *Nature* 1999; 397:69-72; PMID:9892355; <http://dx.doi.org/10.1038/16264>
4. Shpilka T, Weidberg H, Pietrokovski S, Elazar Z. Atg8: an autophagy-related ubiquitin-like protein family. *Genome Biol* 2011; 12:226; PMID:21867568; <http://dx.doi.org/10.1186/gb-2011-12-7-226>
5. Mansuy V, Boireau W, Fraichard A, Schlick JL, Jouvenot M, Delage-Mourroux R. GEC1, a protein related to GABARAP, interacts with tubulin and GABA(A) receptor. *Biochem Biophys Res Commun* 2004; 325:639-48; PMID:15530441; <http://dx.doi.org/10.1016/j.bbrc.2004.10.072>
6. Chen C, Li JG, Chen Y, Huang P, Wang Y, Liu-Chen LY. GEC1 interacts with the kappa opioid receptor and enhances expression of the receptor. *J Biol Chem* 2006; 281:7983-93; PMID:16431922; <http://dx.doi.org/10.1074/jbc.M509805200>
7. Mansuy-Schlick V, Tolle F, Delage-Mourroux R, Fraichard A, Risold PY, Jouvenot M. Specific distribution of gabarap, gec1/gabarap Like 1, gate16/gabarap Like 2, lc3 messenger RNAs in rat brain areas by quantitative real-time PCR. *Brain Res* 2006; 1073-1074:83-7; PMID:16458273; <http://dx.doi.org/10.1016/j.brainres.2005.11.004>
8. Tolle F, Risold PY, Mansuy-Schlick V, Rossi E, Boyer-Guittaut M, Fraichard A, Jouvenot M. Specific regional distribution of gec1 mRNAs in adult rat central nervous system. *Brain Res* 2008; 1210:103-15; PMID:18423580; <http://dx.doi.org/10.1016/j.brainres.2008.02.077>
9. Le Grand JN, Bon K, Fraichard A, Zhang J, Jouvenot M, Risold PY, Boyer-Guittaut M, Delage-Mourroux R. Specific distribution of the autophagic protein GABARAPL1/GEC1 in the developing and adult mouse brain and identification of neuronal populations expressing GABARAPL1/GEC1. *PLoS One* 2013; 8:e63133; PMID:23690988; <http://dx.doi.org/10.1371/journal.pone.0063133>
10. Sengupta A, Molkentin JD, Yutzev KE. FoxO transcription factors promote autophagy in cardiomyocytes. *J Biol Chem* 2009; 284:28319-31; PMID:19696026; <http://dx.doi.org/10.1074/jbc.M109.024406>
11. Jamart C, Benoît N, Raymackers JM, Kim HJ, Kim CK, Francaux M. Autophagy-related and autophagy-regulatory genes are induced in human muscle after ultraendurance exercise. *Eur J Appl Physiol* 2012; 112:3173-7; PMID:22194006; <http://dx.doi.org/10.1007/s00421-011-2287-3>
12. Nemos C, Mansuy V, Vernier-Magnin S, Fraichard A, Jouvenot M, Delage-Mourroux R. Expression of gec1/GABARAPL1 versus GABARAP mRNAs in human: predominance of gec1/GABARAPL1 in the central nervous system. *Brain Res Mol Brain Res* 2003; 119:216-9; PMID:14625090; <http://dx.doi.org/10.1016/j.molbrainres.2003.09.011>
13. Berthier A, Seguin S, Sascio AJ, Bobin JY, De Laroche G, Datchary J, Saez S, Rodriguez-Lafrasse C, Tolle F, Fraichard A, et al. High expression of gabarapl1 is associated with a better outcome for patients with lymph node-positive breast cancer. *Br J Cancer* 2010; 102:1024-31; PMID:20197771; <http://dx.doi.org/10.1038/sj.bjc.6605568>



14. De Palma C, Morisi F, Cheli S, Pambianco S, Cappello V, Vezzoli M, Rovere-Querini P, Moggio M, Ripolone M, Francolini M, et al. Autophagy as a new therapeutic target in Duchenne muscular dystrophy. *Cell Death Dis* 2012; 3:e418; PMID:23152054; <http://dx.doi.org/10.1038/cddis.2012.159>
15. von Walden F, Jakobsson F, Edström L, Nader GA. Altered autophagy gene expression and persistent atrophy suggest impaired remodeling in chronic hemiplegic human skeletal muscle. *Muscle Nerve* 2012; 46:785-92; PMID:22996233; <http://dx.doi.org/10.1002/mus.23387>
16. Simunovic F, Yi M, Wang Y, Macey L, Brown LT, Krichevsky AM, Andersen SL, Stephens RM, Benes FM, Sonntag KC. Gene expression profiling of substantia nigra dopamine neurons: further insights into Parkinson's disease pathology. *Brain* 2009; 132:1795-809; PMID:19052140; <http://dx.doi.org/10.1093/brain/awn323>
17. Lee J, Giordano S, Zhang J. Autophagy, mitochondria and oxidative stress: cross-talk and redox signaling. *Biochem J* 2012; 441:523-40; PMID:22187934; <http://dx.doi.org/10.1042/BJ20111451>
18. Hill BG, Benavides GA, Lancaster JR Jr., Ballinger S, Dell'Italia L, Jianhua Z, Darley-USmar VM. Integration of cellular bioenergetics with mitochondrial quality control and autophagy. *Biol Chem* 2012; 393:1485-512; PMID:23092819; <http://dx.doi.org/10.1515/hsz-2012-0198>
19. Mitchell T, Chacko B, Ballinger SW, Bailey SM, Zhang J, Darley-USmar V. Convergent mechanisms for dysregulation of mitochondrial quality control in metabolic disease: implications for mitochondrial therapeutics. *Biochem Soc Trans* 2013; 41:127-33; PMID:23356271; <http://dx.doi.org/10.1042/BST20120231>
20. Zhang J. Autophagy and Mitophagy in Cellular Damage Control. *Redox Biol* 2013; 1:19-23; PMID:23946931; <http://dx.doi.org/10.1016/j.redox.2012.11.008>
21. Dodson M, Darley-USmar V, Zhang J. Cellular metabolic and autophagic pathways: traffic control by redox signaling. *Free Radic Biol Med* 2013; 63:207-21; PMID:23702245; <http://dx.doi.org/10.1016/j.freeradbiomed.2013.05.014>
22. Benbrook DM, Long A. Integration of autophagy, proteasomal degradation, unfolded protein response and apoptosis. *Exp Oncol* 2012; 34:286-97; PMID:23070014
23. Yang Z, Klionsky DJ. An overview of the molecular mechanism of autophagy. *Curr Top Microbiol Immunol* 2009; 335:1-32; PMID:19802558; [http://dx.doi.org/10.1007/978-3-642-00302-8\\_1](http://dx.doi.org/10.1007/978-3-642-00302-8_1)
24. Hill BG, Benavides GA, Lancaster JR Jr., Ballinger S, Dell'Italia L, Jianhua Z, Darley-USmar VM. Integration of cellular bioenergetics with mitochondrial quality control and autophagy. *Biol Chem* 2012; 393:1485-512; PMID:23092819; <http://dx.doi.org/10.1515/hsz-2012-0198>
25. Higdon A, Diers AR, Oh JY, Landar A, Darley-USmar VM. Cell signalling by reactive lipid species: new concepts and molecular mechanisms. *Biochem J* 2012; 442:453-64; PMID:22364280; <http://dx.doi.org/10.1042/BJ20111752>
26. Weidberg H, Shvets E, Shpilka T, Shimron F, Shinder V, Elazar Z. LC3 and GATE-16/GABARAP subfamilies are both essential yet act differently in autophagosome biogenesis. *EMBO J* 2010; 29:1792-802; PMID:20418806; <http://dx.doi.org/10.1038/emboj.2010.74>
27. Cann GM, Guignabert C, Ying L, Deshpande N, Bekker JM, Wang L, Zhou B, Rabinovitch M. Developmental expression of LC3alpha and beta: absence of fibronectin or autophagy phenotype in LC3beta knockout mice. *Dev Dyn* 2008; 237:187-95; PMID:18069693; <http://dx.doi.org/10.1002/dvdy.21392>
28. O'Sullivan GA, Kneussel M, Elazar Z, Betz H. GABARAP is not essential for GABA receptor targeting to the synapse. *Eur J Neurosci* 2005; 22:2644-8; PMID:16307606; <http://dx.doi.org/10.1111/j.1460-9568.2005.04448.x>
29. Chen ZH, Lam HC, Jin Y, Kim HP, Cao J, Lee SJ, Ifedigbo E, Parameswaran H, Ryter SW, Choi AM. Autophagy protein microtubule-associated protein 1 light chain-3B (LC3B) activates extrinsic apoptosis during cigarette smoke-induced emphysema. *Proc Natl Acad Sci U S A* 2010; 107:18880-5; PMID:20956295; <http://dx.doi.org/10.1073/pnas.1005574107>
30. Shaid S, Brandts CH, Serve H, Dikic I. Ubiquitination and selective autophagy. *Cell Death Differ* 2013; 20:21-30; PMID:22722335; <http://dx.doi.org/10.1038/cdd.2012.72>
31. Novak I, Kirkin V, McEwan DG, Zhang J, Wild P, Rozenknop A, Rogov V, Löhr F, Popovic D, Occhipinti A, et al. Nix is a selective autophagy receptor for mitochondrial clearance. *EMBO Rep* 2010; 11:45-51; PMID:20010802; <http://dx.doi.org/10.1038/embor.2009.256>
32. Jiang S, Heller B, Tagliabracchi VS, Zhai L, Irimia JM, DePaoli-Roach AA, Wells CD, Skurat AV, Roach PJ. Starch binding domain-containing protein 1/genothinin 1 is a novel participant in glycogen metabolism. *J Biol Chem* 2010; 285:34960-71; PMID:20810658; <http://dx.doi.org/10.1074/jbc.M110.150839>
33. Jiang S, Wells CD, Roach PJ. Starch-binding domain-containing protein 1 (Stbd1) and glycogen metabolism: Identification of the Atg8 family interacting motif (AIM) in Stbd1 required for interaction with GABARAPL1. *Biochem Biophys Res Commun* 2011; 413:420-5; PMID:21893048; <http://dx.doi.org/10.1016/j.bbrc.2011.08.106>
34. Zhang Y, Wang F, Han L, Wu Y, Li S, Yang X, Wang Y, Ren F, Zhai Y, Wang D, et al. GABARAPL1 negatively regulates Wnt/ $\beta$ -catenin signaling by mediating Dvl2 degradation through the autophagy pathway. *Cell Physiol Biochem* 2011; 27:503-12; PMID:21691068; <http://dx.doi.org/10.1159/000329952>
35. Debnath J. The multifaceted roles of autophagy in tumors-implications for breast cancer. *J Mammary Gland Biol Neoplasia* 2011; 16:173-87; PMID:21779879; <http://dx.doi.org/10.1007/s10911-011-9223-3>
36. Arduíno DM, Esteves AR, Cortes L, Silva DF, Patel B, Grazina M, Swerdlow RH, Oliveira CR, Cardoso SM. Mitochondrial metabolism in Parkinson's disease impairs quality control autophagy by hampering microtubule-dependent traffic. *Hum Mol Genet* 2012; 21:4680-702; PMID:22843496; <http://dx.doi.org/10.1093/hmg/dds309>
37. Ishii T, Warabi E, Siow RC, Mann GE. Sequestosome1/p62: a regulator of redox-sensitive voltage-activated potassium channels, arterial remodeling, inflammation, and neurite outgrowth. *Free Radic Biol Med* 2013; 65:102-16; PMID:23792273; <http://dx.doi.org/10.1016/j.freeradbiomed.2013.06.019>
38. Liang Q, Benavides GA, Vassilopoulos A, Gius D, Darley-USmar V, Zhang J. Bioenergetic and autophagic control by Sirt3 in response to nutrient deprivation in mouse embryonic fibroblasts. *Biochem J* 2013; 454:249-57; PMID:23767918; <http://dx.doi.org/10.1042/BJ20130414>
39. Kurzawa-Akanbi M, Hanson PS, Blain PG, Lett DJ, McKeith IG, Chinnery PF, Morris CM. Glucocerebrosidase mutations alter the endoplasmic reticulum and lysosomes in Lewy body disease. *J Neurochem* 2012; 123:298-309; PMID:22803570; <http://dx.doi.org/10.1111/j.1471-4159.2012.07879.x>
40. Dranka BP, Benavides GA, Diers AR, Giordano S, Zelickson BR, Reily C, Zou L, Chatham JC, Hill BG, Zhang J, et al. Assessing bioenergetic function in response to oxidative stress by metabolic profiling. *Free Radic Biol Med* 2011; 51:1621-35; PMID:21872656; <http://dx.doi.org/10.1016/j.freeradbiomed.2011.08.005>
41. Schneider L, Giordano S, Zelickson BR, S Johnson M, A Benavides G, Ouyang X, Fineberg N, Darley-USmar VM, Zhang J. Differentiation of SH-SY5Y cells to a neuronal phenotype changes cellular bioenergetics and the response to oxidative stress. *Free Radic Biol Med* 2011; 51:2007-17; PMID:21945098; <http://dx.doi.org/10.1016/j.freeradbiomed.2011.08.030>
42. Meirhaeghe A, Crowley V, Lenaghan C, Lelliott C, Green K, Stewart A, Hart K, Schinner S, Sethi JK, Yeo G, et al. Characterization of the human, mouse and rat PGC1 beta (peroxisome-proliferator-activated receptor-gamma co-activator 1 beta) gene in vitro and in vivo. *Biochem J* 2003; 373:155-65; PMID:12678921; <http://dx.doi.org/10.1042/BJ20030200>
43. Shoshan-Barmatz V, Mizrahi D. VDAC1: from structure to cancer therapy. *Front Oncol* 2012; 2:164; PMID:23233904; <http://dx.doi.org/10.3389/fonc.2012.00164>
44. Chen H, Chan DC. Physiological functions of mitochondrial fusion. *Ann N Y Acad Sci* 2010; 1201:21-5; PMID:20649534; <http://dx.doi.org/10.1111/j.1749-6632.2010.05615.x>
45. Blackstone C, Chang CR. Mitochondria unite to survive. *Nat Cell Biol* 2011; 13:521-2; PMID:21540850; <http://dx.doi.org/10.1038/ncb0511-521>
46. Ashrafi G, Schwarz TL. The pathways of mitophagy for quality control and clearance of mitochondria. *Cell Death Differ* 2013; 20:31-42; PMID:22743996; <http://dx.doi.org/10.1038/cdd.2012.81>
47. Sansbury BE, Jones SP, Riggs DW, Darley-USmar VM, Hill BG. Bioenergetic function in cardiovascular cells: the importance of the reserve capacity and its biological regulation. *Chem Biol Interact* 2011; 191:288-95; PMID:21147079; <http://dx.doi.org/10.1016/j.cbi.2010.12.002>
48. Guo J, Prokai-Tatrai K, Nguyen V, Rauniyar N, Ughy B, Prokai L. Protein targets for carbonylation by 4-hydroxy-2-nonenal in rat liver mitochondria. *J Proteomics* 2011; 74:2370-9; PMID:21801862; <http://dx.doi.org/10.1016/j.jpropt.2011.07.009>
49. Fritz KS, Galligan JJ, Smathers RL, Roede JR, Shearn CT, Reigan P, Petersen DR. 4-Hydroxynonenal inhibits SIRT3 via thiol-specific modification. *Chem Res Toxicol* 2011; 24:651-62; PMID:21449565; <http://dx.doi.org/10.1021/tx100355a>
50. Falletti O, Douki T. Low glutathione level favors formation of DNA adducts to 4-hydroxy-2(E)-nonenal, a major lipid peroxidation product. *Chem Res Toxicol* 2008; 21:2097-105; PMID:18847228; <http://dx.doi.org/10.1021/tx800169a>
51. Klebig C, Seitz S, Arnold W, Deutschmann N, Pacyna-Gengelbach M, Scherneck S, Petersen I. Characterization of gamma-aminobutyric acid type A receptor-associated protein, a novel tumor suppressor, showing reduced expression in breast cancer. *Cancer Res* 2005; 65:394-400; PMID:15695379
52. Lock R, Roy S, Kenific CM, Su JS, Salas E, Ronen SM, Debnath J. Autophagy facilitates glycolysis during Ras-mediated oncogenic transformation. *Mol Biol Cell* 2011; 22:165-78; PMID:21119005; <http://dx.doi.org/10.1091/mbc.E10-06-0500>
53. Carew JS, Kelly KR, Nawrocki ST. Autophagy as a target for cancer therapy: new developments. *Cancer Manag Res* 2012; 4:357-65; PMID:23091399
54. Sarkar S, Davies JE, Huang Z, Tunnacliffe A, Rubinsztein DC. Trehalose, a novel mTOR-independent autophagy enhancer, accelerates the clearance of mutant huntingtin and alpha-synuclein. *J Biol Chem* 2007; 282:5641-52; PMID:17182613; <http://dx.doi.org/10.1074/jbc.M609532200>

55. Dehay B, Bové J, Rodríguez-Muela N, Perier C, Recasens A, Boya P, Vila M. Pathogenic lysosomal depletion in Parkinson's disease. *J Neurosci* 2010; 30:12535-44; PMID:20844148; <http://dx.doi.org/10.1523/JNEUROSCI.1920-10.2010>
56. Chauhan S, Goodwin JG, Chauhan S, Manyam G, Wang J, Kamat AM, Boyd DD. ZKSCAN3 is a master transcriptional repressor of autophagy. *Mol Cell* 2013; 50:16-28; PMID:23434374; <http://dx.doi.org/10.1016/j.molcel.2013.01.024>
57. Künzli N. Happy birthday MPH (Master of Public Health): it's time for the party--a reality check and a cure. *Soz Präventivmed* 2002; 47:279-80; PMID:12512220; <http://dx.doi.org/10.1007/PL00012636>
58. Ohri SS, Vashishta A, Proctor M, Fusek M, Vetvicka V. The propeptide of cathepsin D increases proliferation, invasion and metastasis of breast cancer cells. *Int J Oncol* 2008; 32:491-8; PMID:18202773
59. Chen QY, Shi JG, Yao QH, Jiao DM, Wang YY, Hu HZ, Wu YQ, Song J, Yan J, Wu LJ. Lysosomal membrane permeabilization is involved in curcumin-induced apoptosis of A549 lung carcinoma cells. *Mol Cell Biochem* 2012; 359:389-98; PMID:21874542; <http://dx.doi.org/10.1007/s11010-011-1033-9>
60. Rudd LP, Kabler SL, Morrow CS, Townsend AJ. Enhanced glutathione depletion, protein adduct formation, and cytotoxicity following exposure to 4-hydroxy-2-nonenal (HNE) in cells expressing human multidrug resistance protein-1 (MRP1) together with human glutathione S-transferase-M1 (GSTM1). *Chem Biol Interact* 2011; 194:113-9; PMID:21925487; <http://dx.doi.org/10.1016/j.cbi.2011.08.012>
61. Dickinson DA, Levenon AL, Moellering DR, Arnold EK, Zhang H, Darley-Usmar VM, Forman HJ. Human glutamate cysteine ligase gene regulation through the electrophile response element. *Free Radic Biol Med* 2004; 37:1152-9; PMID:15451055; <http://dx.doi.org/10.1016/j.freeradbiomed.2004.06.011>
62. Tietze F. Enzymic method for quantitative determination of nanogram amounts of total and oxidized glutathione: applications to mammalian blood and other tissues. *Anal Biochem* 1969; 27:502-22; PMID:4388022; [http://dx.doi.org/10.1016/0003-2697\(69\)90064-5](http://dx.doi.org/10.1016/0003-2697(69)90064-5)
63. Knight-Lozano CA, Young CG, Burow DL, Hu ZY, Uyeminami D, Pinkerton KE, Ischiropoulos H, Ballinger SW. Cigarette smoke exposure and hypercholesterolemia increase mitochondrial damage in cardiovascular tissues. *Circulation* 2002; 105:849-54; PMID:11854126; <http://dx.doi.org/10.1161/hc0702.103977>
64. Westbrook DG, Anderson PG, Pinkerton KE, Ballinger SW. Perinatal tobacco smoke exposure increases vascular oxidative stress and mitochondrial damage in non-human primates. *Cardiovasc Toxicol* 2010; 10:216-26; PMID:20668962; <http://dx.doi.org/10.1007/s12012-010-9085-8>
65. Mitchell T, Johnson MS, Ouyang X, Chacko BK, Mitra K, Lei X, Gai Y, Moore DR, Barnes S, Zhang J, et al. Dysfunctional mitochondrial bioenergetics and oxidative stress in Akita(+Ins2)-derived  $\beta$ -cells. *Am J Physiol Endocrinol Metab* 2013; 305:E585-99; PMID:23820623; <http://dx.doi.org/10.1152/ajpendo.00093.2013>